Perturbed orbital motion of regolith around Asteroids

MSc Thesis Report

Abhishek Agrawal

TUDelft
Delft
University of
Technology

PERTURBED ORBITAL MOTION OF REGOLITH AROUND ASTEROIDS

MSc Thesis Report

by

ABHISHEK AGRAWAL

to obtain the degree of Master of Science
at the Delft University of Technology.

TUDelft

"If you wish to make an apple pie from scratch, you must first invent the universe."
Carl Sagan

PREFACE

After 45 years since the day man landed on the Moon, mankind created history, yet again. For the first time ever, a spacecraft was put into an orbit around a comet and a lander was deployed to its surface. This was the Rosetta mission; launched in March 2004, the spacecraft took an astonishing 10 years to travel to the comet 67P/Churyumov-Gerasimenko, finally arriving at the comet in August 2014. This is an immense achievement for the scientists and engineers involved in the Rosetta mission because space missions to small irregular bodies in our solar system, both comets and asteroids, pose significant dynamical challenges. For scientists, missions to comets and asteroids are of great interest since in-situ exploration of these small bodies can provide insight into the birth of our Solar System and answer some very important and fundamental questions such as those about the origins of life on Earth. Now even the private space industry is interested in these small bodies, such as in mining the vast reserves of untapped natural resources within the small bodies. For a student, designing and assessing orbits around a small irregular body, and in our case an asteroid, turns out to be one of the toughest problems in astrodynamics, making it a perfect research topic for an MSc Thesis.

This report serves to be a *Literature Study* in the framework of the Master's program at the Faculty of Aerospace Engineering, Delft University of Technology. It paves way for the upcoming thesis project, where the actual research work shall be carried out. I am grateful I could do this literature study under the supervision of my supervisor Ir. Ron Noomen and with support from Dr. Jinglang Feng. Their experience in the subject matter has been of tremendous help to me. In writing this report, I have tried my very best to ensure that the material in the report is presented in a manner which is pleasant to read and understand. I hope you can gain some valuable knowledge from reading this report.

Abhishek Agrawal
Delft, August 2016

CONTENTS

LIST OF SYMBOLS

LATIN LETTERS

Symbol	Units	Description
r	m	position vector magnitude
$\mathbf{r}$	m	position vector
U	m^2/s^2	Gravitational potential

GREEK

Symbol	Units	Description
α	m	Largest semi-major axis of tri-axial ellipsoid shaped asteroid

LIST OF ACRONYMS

AU Astronomical Unit

CCW Counter-Clockwise

EHAO Extremely-High Altitude Orbit

HAO High Altitude Orbit

LAO Low Altitude Orbit

MAO Medium Altitude Orbit

MBO Main-Belt Objects

NEA Near-Earth Asteroids

NEAR Near Earth Asteroid Rendezvous

SRP Solar Radiation Pressure

STBE Solar Third Body Effect

TNO Trans-Neptunian Objects

UHAO Ultra-High Altitude Orbit

1

INTRODUCTION

Asteroids are small rocky bodies in our solar system that are orbiting the Sun. These small bodies are basically the remnants from the process that formed the inner planets in our Solar System (*Jet Propulsion Laboratory, Why Study Asteroids?*). Asteroids are mainly found in an orbit between Jupiter and Mars and as such are classified as MBO (Main-Belt Objects). These MBO range in size from a few meters to hundreds of kilometers, the largest one being 1 Ceres with a diameter of 948 km. A subset of the MBO, called the NEA (Near-Earth Asteroids), are asteroids whose orbits come extremely close to, and sometimes even cross, the orbit of the Earth (*Jet Propulsion Laboratory, Solar System dynamics, Asteroids*). Other small bodies in our small system, classified as asteroids when broadly speaking, are the Trojans (small bodies captured at Jupiter's Lagrange points 4 and 5), the TNO (Trans-Neptunian Objects) (small bodies whose orbits around the Sun go beyond Neptune), the Centaurs (small bodies whose orbits lie in between Jupiter and Neptune) (*Jet Propulsion Laboratory, Solar System dynamics, Asteroids*). The asteroids in the main-belt tend to be more rocky in nature, however the small bodies beyond Jupiter tend to have a more icy-composition due to their relatively larger distance from the Sun (*Jet Propulsion Laboratory, Solar System dynamics, Asteroids*). A histogram plot depicting the distribution of MBO is shown in Figure 1.1. The gaps in the plot depict resonance in mean-motion between Jupiter and an asteroid (*Jet Propulsion Laboratory, Solar System dynamics, Asteroids*).

Asteroids don't only exist as single bodies in the Solar System, but they are also found in local multi-body systems consisting of two to even three asteroids. With advanced asteroid detection methods, astrophysicists have found over 190 multiple asteroid systems in the Solar System (Marchis et al. 2012). Contrary to intuition, these multiple asteroid systems exhibit a wide diversity in terms of the size ratios of the components, their mutual orbits and separation, implicating that the individual components evolved differently over time (Marchis et al. 2012). If a multi-asteroid system consists of two or three components, which are bound gravitationally, then it is termed as *binary asteroids* or *triple asteroids* respectively. Triple asteroids are also sometimes termed as *trinary* or *ternary* (Margot et al. 2015). Asteroid components that are not gravitationally bound but are genetically related, are termed as *asteroid pairs*. Asteroid pairs where the larger asteroid is a binary or a triple asteroid, are termed as *paired binaries* or *paired triples*, respectively. The larger component in a binary or triple asteroid system or an asteroid pair, is referred to as the *primary* and similarly the smaller component is referred to as the *secondary* (Margot et al. 2015). Asteroids are further classified based on their dimensions and thermal properties, for which the reader should read the publication in (Marchis et al. 2012).

We now know what asteroids are and the different ways in which they are found in our Solar System, but is it important to study them? There are three major, and most commonly expressed, reasons to study asteroids in our solar system, and not just from a distance such as through radar
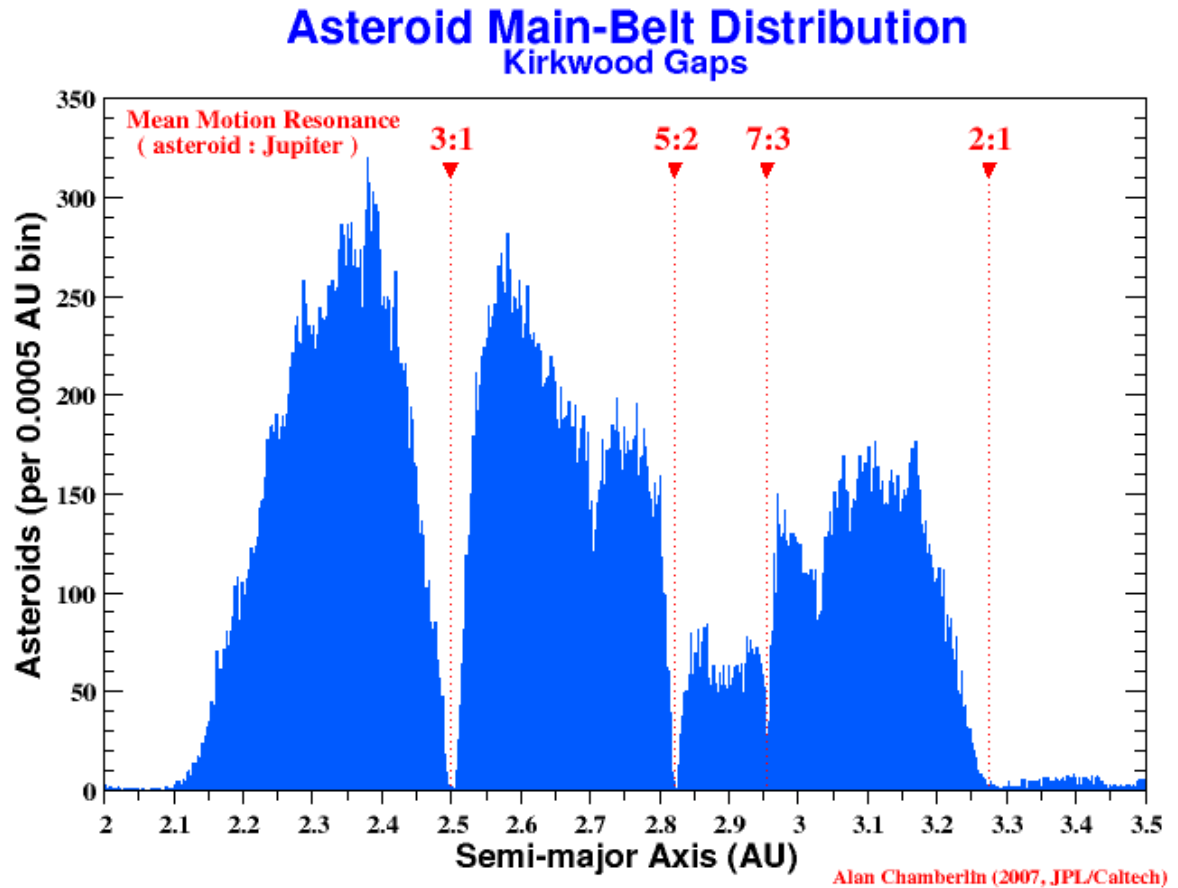
Figure 1.1: Histogram plot depicting distribution of semi-major axis of 156,929 main-belt asteroids, created in June 2007 (*Jet Propulsion Laboratory, Solar System dynamics, Asteroids*).

telescopes placed on Earth, but also through in-situ exploration involving spacecrafts and surface probes. These reasons are mentioned as follows.

- Asteroids are basically the material left-over from formation of planets in our Solar System. Thus, they are the perfect source to study and understand the origins of the Solar System, as they have remained in the same pristine form since the birth of the Solar System, unlike the planets which have undergone massive topographical and atmospheric changes after their formation. The asteroids can provide valuable information on the chemical composition and initial conditions which led to the formation of planets, including Earth some 4.6 billion years ago. Several scientists have also hypothesized that water and life could have been brought about on Earth through an asteroid or comet and hence exploration of these small bodies could provide a definite answer to an age old question of how life began on Earth (*Jet Propulsion Laboratory, Why Study Asteroids?*).

- Asteroids have been hypothesized to have brought complex molecules to the surface of Earth that eventually resulted in life, but lately they have also been linked to the extinction of dinosaurs due to its impact with Earth. Earth is continuously bombarded with very small interplanetary material, most of which doesn't reach the surface of the Earth but gets evaporated in its atmosphere. However, every few 100 years, an asteroid spanning some tens of meter could impact Earth resulting in widespread damage, in the present case to life and property. But the impact from those will not cause the human race to extinct. But every 100,000 years or

so, larger asteroids, spanning over tens of kilometer would impact the Earth, which will lead to extinction of life as we know it now. Although the probability of getting hit by an asteroid on such a large scale is low, it is still a statistical possibility and to be able to device strategies for active deflection of such asteroids, it is imperative that we understand more of the dynamics, properties and composition of the asteroids (*Jet Propulsion Laboratory, Why Study Asteroids?*).

- The third most important reason for us to study asteroids, is the fact that these small bodies are rich in raw materials or minerals. NEA can be exploited for the resources that they possess and use it to build space structures or generate fuel for spacecrafts to enable human space exploration in farther reaches of the Solar System. By studying the asteroids, we can develop methods to tap the vast reservoirs of raw materials residing in them (*Jet Propulsion Laboratory, Why Study Asteroids?*).

Part I

Motivation

2

HERITAGE

3

THESIS OBJECTIVES

Part II

Numerical Simulation Results

4

RESULTS

4.1 REGOLITH LAUNCHED FROM THE LONGEST EDGE OF THE ASTEROID

The results that we'll discuss in this section pertain to the case of regolith launched from the longest edge of the asteroid, modeled as an ellipsoid.

4.1.1 DYNAMICS WITHOUT SOLAR PERTURBATIONS

...to be added later...

4.1.2 DYNAMICS WITH SOLAR PERTURBATIONS

In this case, the simulation accounted for perturbations from the irregular gravity field of the asteroid, the SRP (Solar Radiation Pressure), and the STBE (Solar Third Body Effect). Within this category, there are 4 distinct sets of simulations, each for a particle with different Area-to-Mass ratio. These are mentioned in Table 4.1. The material with a density of 3.2 [g/cm^3] is low-density Olivine (Magnesium Iron Silicates) and the one with 7.5 [g/cm^3] is Iron-Nickel alloy (Garcia-Yarnoz et al. 2014). We have chosen these two types of materials based on the surface composition analysis of asteroid Eros, an S-Type asteroid, from the NEAR (Near Earth Asteroid Rendezvous)-Shoemaker data. S-Type asteroids, from reflectance spectral analysis, are commonly known to have minerals like Olivine, Pyroxene, and Fe-Ni (Iron-Nickel) metal (Nittler et al. 2001). Thermo-spectral analysis of regolith on Eros reveals that it is rich in Olivine and is found to be more abundant than Pyroxene (McCoy et al. 2001). The mineral Olivine has also been discovered on Itokawa, another S-Type asteroid, through transmission electron microscope analysis of samples returned by the Hayabusa spacecraft (Keller et al. 2014). Eros also contains Fe-Ni but it is significantly separated from the Silicates (Olivine and Pyroxene) within the regolith (Nittler et al. 2001). Evans et al. 2001 analyzed elemental composition of NEAR-Shoemaker's landing site on Eros, based on which, it presents several arguments for relatively lower abundance of Fe (Iron) on the surface of Eros. One of the arguments hypothesizes that different grain sizes and density of Fe-Ni from Olivine could have resulted in the metal to get separated from the Silicates, either spatially or for it to sink down in the lower depths of the regolith. In light of this, we are considering regolith comprising of only Olivine and Fe-Ni, to distinguish between their orbital behavior and final fate upon being lofted from the surface of Eros. Veverka et al. 2001 analyzed high resolution surface images of Eros captured by NEAR-Shoemaker on a low-altitude flyover. It argued the build-up of a heterogeneous and complex regolith that comprised of material ranging from fine particles all the way up to metre-sized ejecta blocks. Because of this, in Table 4.1, we have considered coarser regolith since their existence is possible.

13

<div align="center">**Table 4.1:** Particle Area-to-Mass ratios</div>

Code	Particle radius [cm]	Density [g/cm^3]	Area-to-Mass ratio [m^2/kg]
LoGSP-1	1.0	3.2	0.0234
LoGSP-2	1.0	7.5	0.01
LoGSP-3	5.0	3.2	0.0047
LoGSP-4	5.0	7.5	0.002

For each of the four types of particles mentioned in Table 4.1, the initial conditions for lofting the regolith are varied in the same manner. These initial conditions are mentioned as follows. The asteroid revolves around the Sun in an equatorial circular orbit at a distance of 1.0 AU (Astronomical Unit). Four different initial Solar phase angles were considered for the simulation – 45.0, 135.0, 225.0 315.0 [deg], to account for the four different quadrants where the Sun could be with respect to the asteroid. For each case in Table 4.1, a total of 72 particles were launched from the surface of the asteroid, each in a different direction (defined using the launch declination and azimuth angles). The launch declination angle, measured from the zenith, was kept constant at 45.0 [deg] for all the particles. The launch azimuth, measured CCW (Counter-Clockwise) from the direction pointing to north, was varied at a resolution of 5.0 [deg] starting from 0.0 [deg] all the way up to 355.0 [deg]. Each particle was launched, in their specified direction, with different velocities ranging from 1.0 [m/s] to 16.0 [m/s] (measured with respect to the asteroid-centric rotating frame) at a resolution of 1.0 [m/s]. So basically, every combination of an initial Solar phase angle, initial launch azimuth, and initial launch velocity corresponds to a unique trajectory for a single particle of a given Area-to-Mass ratio; Thus amounting to a total of 4608 unique trajectories. The simulations were subjected to run for a maximum of 270.0 [days] and were terminated earlier if a particular trajectory resulted in escape or surface re-impact.

CASE LoGSP-1

The density of the regolith was considered to be 3.2 [g/cm^3] with a spherical shape of radius 1.0 [cm]. Figure 4.1 gives a distribution of particles for each of the three different final fates for the regolith i.e. capture, re-impact, and escape, for different initial launch velocities and initial Solar phase angles. Irrespective of the initial Solar phase, initial launch velocities from 1.0 to 3.0 [m/s] results in particles launched in all directions to eventually re-impact the asteroid's surface. Similarly, for initial launch velocities ranging from 14.0 to 16.0 [m/s], we see that the particles always manage to escape the gravitational attraction of the asteroid. However, there is one exception to the former statement, a single particle launched with a velocity of 14.0 [m/s] at a launch azimuth of 90.0 [deg] and at an initial Solar phase angle of 315.0 [deg], re-impacts the asteroid's surface. It is interesting to note that the launch azimuth of the particle is such that it is launched in a direction that is directly opposite to the direction of rotation of the asteroid. Launch velocities from 4.0 to 13.0 [m/s] show a mixed behavior and the final fate distribution trend does not vary drastically for different initial Solar phase angles.

The number of capture cases is far less than those for escape and re-impact. For initial Solar phase of 225.0 [deg], there are no cases of regolith being captured in orbit around the asteroid. All capture cases, arranged in order of increasing launch azimuth angle, are listed in Table 4.2. It is interesting to note that all capture cases result from when the particle is launched in a direction which is against the direction of rotation of the asteroid, bar one exception which is case index-11 in Table 4.2. The capture cases which represent symmetry in terms of the launch azimuth angle are highlighted with the same color in Table 4.2. This symmetric behavior results from the combination of two factors. First, the Sun's motion relative to the asteroid is not in an inclined plane, and secondly, the particles are launched from the equatorial tip of the ellipsoid shaped asteroid, which is a point of symmetry on the ellipsoid. The capture cases will be discussed in detail a bit further ahead.

Table 4.2: Initial conditions that resulted in temporary orbital capture of regolith around the asteroid. Particle code LoGSP-1.

Index	Launch azimuth [deg]	Launch velocity [m/s]	Initial Solar phase angle [deg]
1	5.0	5.0	315.0
2	10.0	9.0	135.0
3	15.0	8.0	45.0
4	45.0	12.0	45.0
5	45.0	10.0	315.0
6	135.0	12.0	45.0
7	135.0	10.0	315.0
8	165.0	8.0	45.0
9	170.0	9.0	135.0
10	175.0	5.0	315.0
11	185.0	5.0	135.0
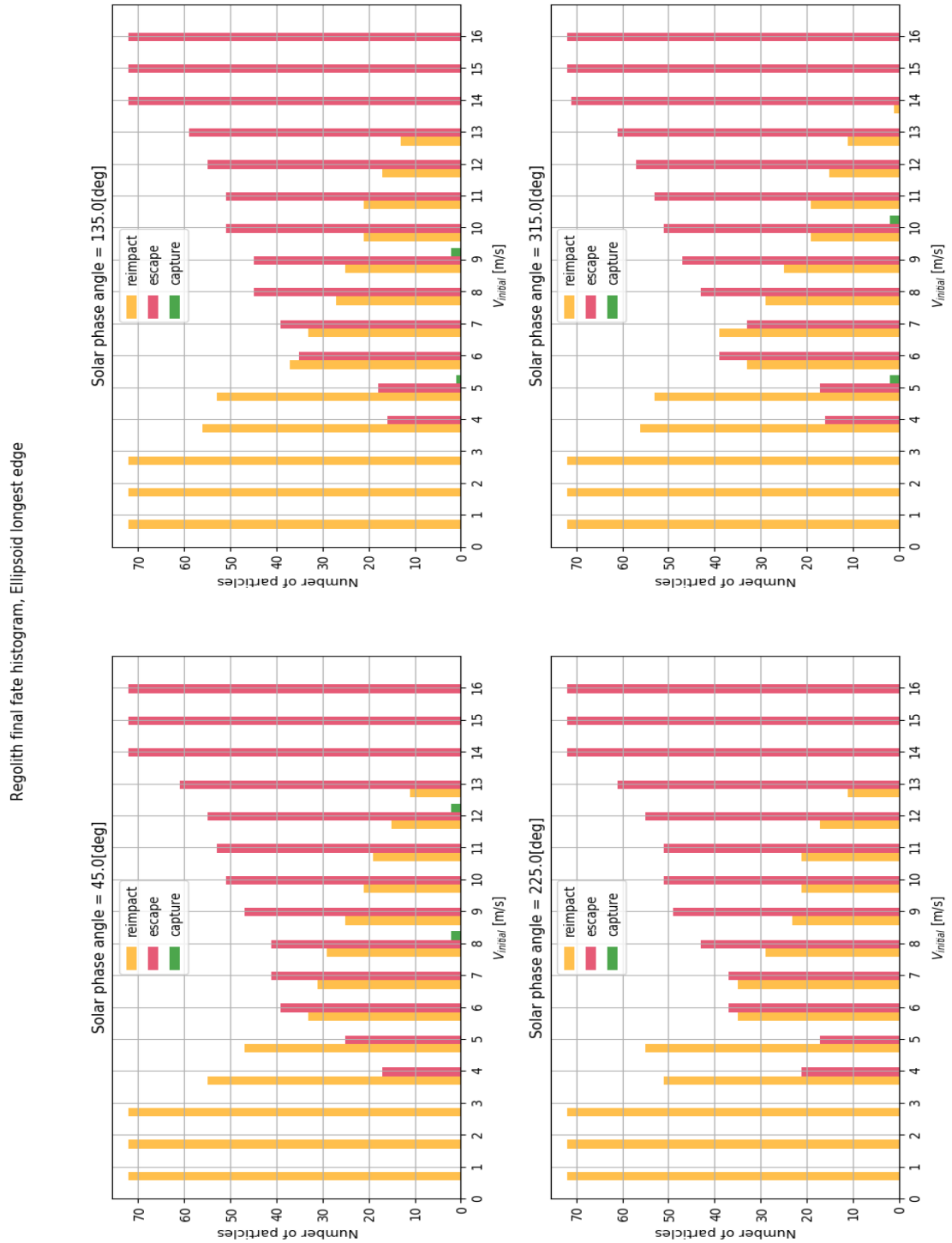
Figure 4.1: Histogram showing the number of particles that re-impact, escape, or get captured around the asteroid, for different initial launch velocities. Particle code LoGSP-1.

Figure 4.2 depicts the surface distribution of regolith that re-impacts the surface when launched from the same location with different velocities and different initial Solar phase angles. The launch location is in the centre of the map, Latitude 0.0 [deg] and Longitude 0.0 [deg]. The particle distribution is the same for regions close to the launch point and for lower launch velocities up until 8.0 [m/s]. A similarity in distribution pattern is also observed around Longitude -150.0 [deg] for launch velocity of 9.0 [m/s] and around Longitude 150.0 [deg] for launch velocity of 10.0 [m/s] for the four Solar phase angles. The distribution pattern, for all launch velocities and initial Solar phases, is also symmetric about the equator. Again, the reason for this is the same as mentioned earlier for the symmetry in capture cases in Table 4.2. Keeping the launch direction and velocity constant, we see that the distribution of regolith that re-impacts the surface does not change drastically with varying initial Solar phase angles, except for a relatively few cases. This is much easily observed in a plot of Range from the launch direction to the re-impact point versus launch azimuth for different velocities as shown in Figure 4.3.

We haven't shown the range to re-impact point plots in Figure 4.3 for all launch velocities because the intention here is to show the qualitative behavior, which can be achieved by considering only a subset of the launch velocities that result in a re-impact scenario. The very first thing we observe is that as the launch velocity increases, the range of launch azimuth over which the regolith re-impacts the surface reduces because a higher velocity allows the regolith to enter a higher orbit (as it attains a relatively higher energy) and reduces the probability of a re-impact. Even as the velocity increases, we see that the azimuths that result in a re-impact are the ones in which the regolith is launched in a direction that is opposite to the asteroid's rotation direction. This makes sense since the regolith's energy would be reduced the most in this scenario compared to all other launch directions, thereby increasing the chances of a re-impact.

Now the primary purpose of the plots in Figure 4.3 (combined with Figure 4.2) is to depict the qualitative effect of Solar perturbations, for varying initial Solar phase angles, on the re-impact behavior of regolith compared to the case when no Solar perturbations are considered. For launch velocities of 4.0, 7.0 and 10.0 [m/s], we see that the Solar perturbations do not affect the re-impact location for cases when the particle is launched in directions opposite to that of the asteroid's rotation. However, we do see few exceptions to the former statement, most noticeably in the case of 7.0 [m/s]. But for the majority of cases where the re-impact location remains unchanged, we see from Figure 4.4, that these particles spend less than 3.0 [Hrs] in orbit which is not enough time for the Solar perturbations to act and have any significant impact on the dynamics of the particles. So in essence this is what's happening here - Particles when launched in a direction that is opposite to that of the asteroid's rotation, even at relatively high velocities such as 10.0 [m/s], loose enough energy to stay in a relatively lower orbit (see Figure A.1) where the gravitational force of the asteroid is significantly stronger than any of the Solar perturbations and as the particle spends a very short time in orbit before re-impact, the Solar perturbations do not get enough time to affect the particle's orbit and hence the particle re-impacts the same location as it would have when no Solar perturbations were considered in the simulation. For the lower launch velocities of 4.0 and 7.0 [m/s], the differences in re-impact locations are more pronounced when the regolith is launched in the same direction as that of the asteroid's rotation. Particles gain relatively higher energy in this case, enter a higher orbit and spend enough time in there for the Solar perturbations to affect it's motion. For the case of the launch velocity of 13.0 [m/s] in Figure 4.3, the velocity is high enough such that the particle does not loose enough energy when launched opposite to the asteroid's rotational direction and is able to enter a relatively higher orbit (see Figure A.1) and stay there for a relatively longer time, as seen in Figure 4.4, which results in the Solar perturbations affecting the orbital motion and eventually the re-impact location of the regolith.
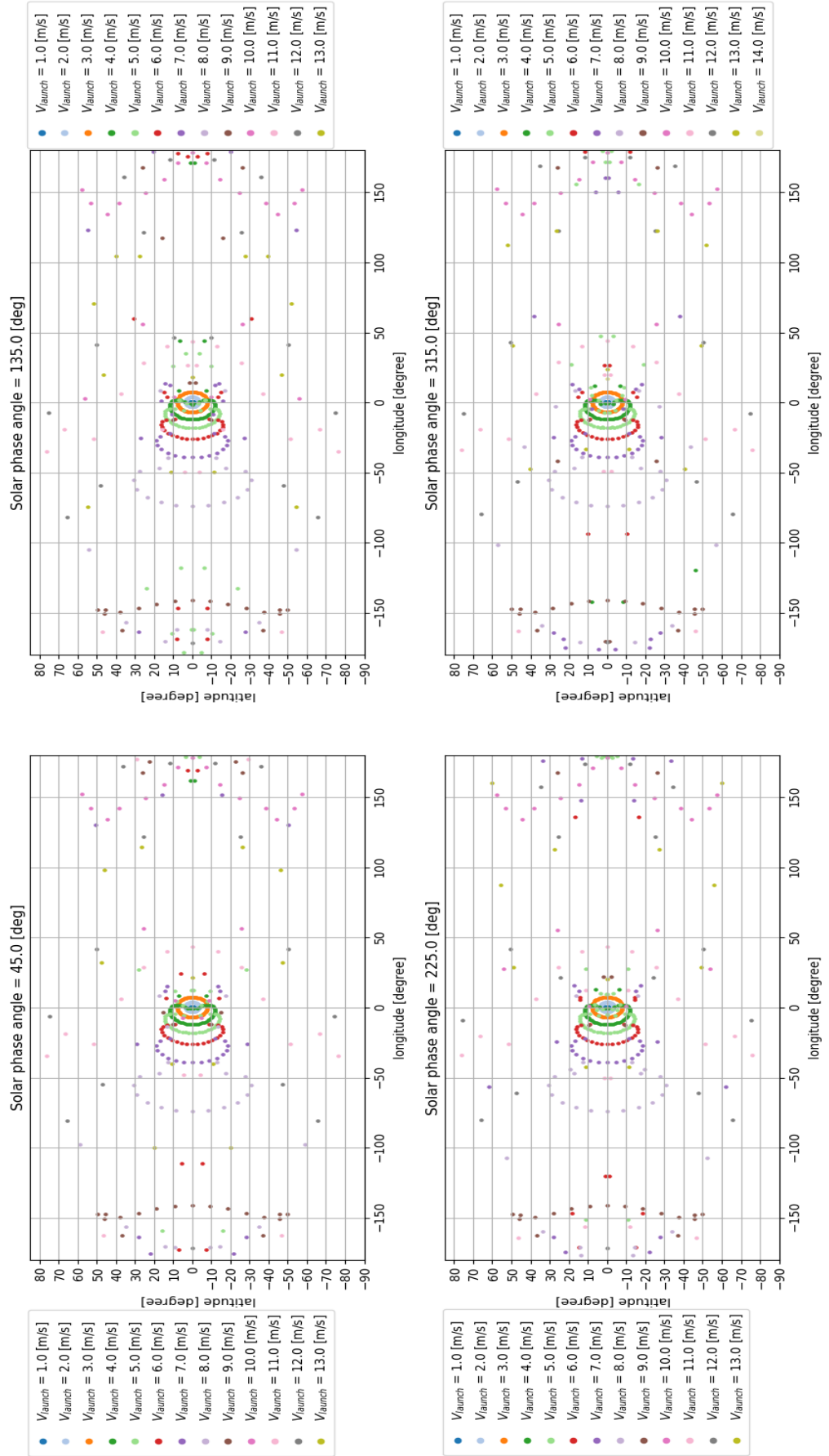
Figure 4.2: Surface distribution of re-impacted regolith for different launch velocities. The launch location is latitude: 0.0 [deg], longitude: 0.0 [deg]. Particle code LoGSP-1.
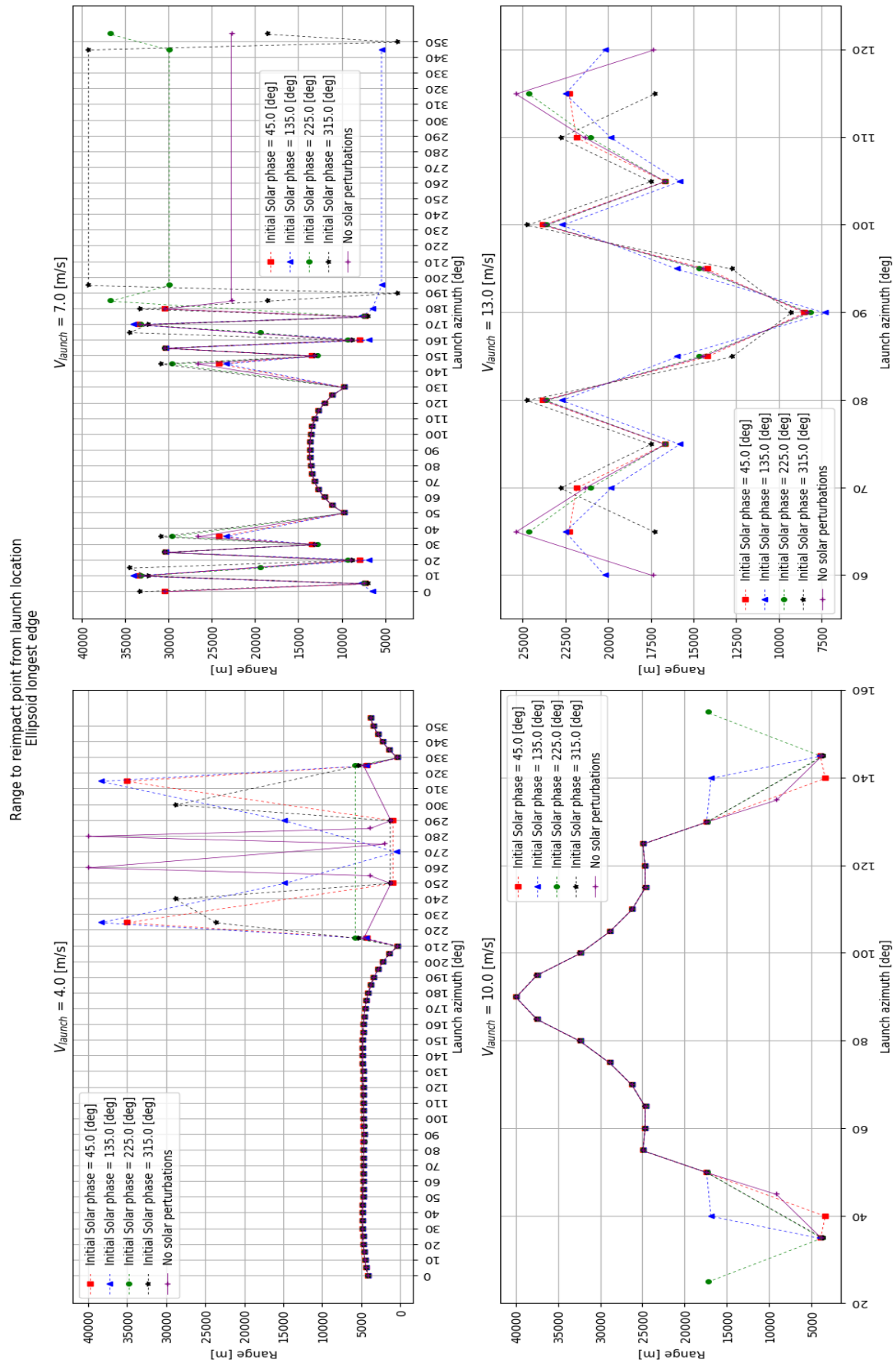
Figure 4.3: Range to re-impact location from the launch point for different velocities. Particle code LoGSP-1.
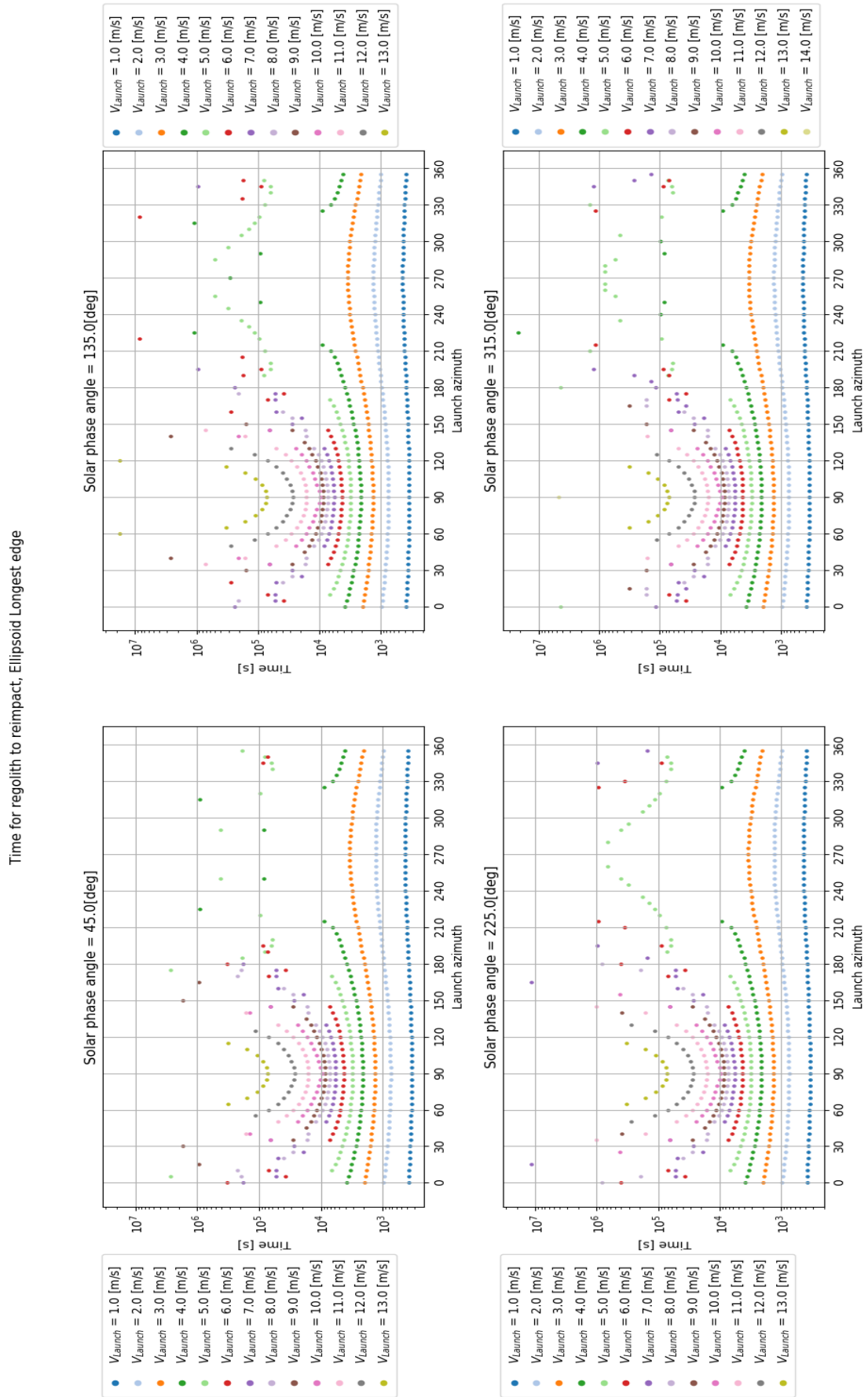
Figure 4.4: Time taken by regolith at different velocities and launch directions to re-impact with the surface of the asteroid. Particle code LoGSP-1.

We shall now look at the cases where the lofted regolith gets (temporarily) captured in orbit by the asteroid. The initial conditions for all capture cases, for the current particle size and density, were mentioned earlier in Table 4.2. Figure 4.6 depicts the progression in orbital range of the temporarily captured regolith. The straight lines in the plot are used to mark the different altitude regimes. These are the LAO (Low Altitude Orbit), MAO (Medium Altitude Orbit), HAO (High Altitude Orbit), UHAO (Ultra-High Altitude Orbit), and EHAO (Extremely-High Altitude Orbit). These altitude regime definitions are not from well defined standards, but instead were arbitrarily chosen as integer multiples of the longest semi-major axis, α, of the tri-axial ellipsoid shaped asteroid. The definition for these altitude regimes is given in Table 4.3.

Table 4.3: Altitude regimes and their definitions

Altitude regime	Definition
LAO	Asteroid surface to $2 \times \alpha$
MAO	$2 \times \alpha$ to $3 \times \alpha$
HAO	$3 \times \alpha$ to $5 \times \alpha$
UHAO	$5 \times \alpha$ to $7 \times \alpha$
EHAO	Above $7 \times \alpha$

The purpose of plotting data as shown in Figure 4.6 was to look for any patterns or periodicity, if they existed, and to see if particles in temporary capture scenario remain closer to the asteroid or further away from it. The symmetry as explained for initial conditions mentioned in Table 4.2 can also be seen in Figure 4.6, for example, regolith launched with velocity of 8.0 [m/s] and launch azimuth of 15.0 [deg] (shown by the purple curve in the top plot in Figure 4.6) shows the same behavior as that of regolith launched with the same velocity and 165.0 [deg] launch azimuth (shown by the green curve in the bottom plot in Figure 4.6). Another thing we see from the plot is that, apart from case number 11 in Table 4.2, the captured regolith stay in the higher altitude regions for most part and only briefly do they fall within the MAO and LAO region. We shall now look at atleast three cases from Figure 4.6 in a bit more detail to understand the effect of Solar perturbations by comparing these cases with their counterparts from the simulation where Solar perturbations were omitted.

Of all the cases shown in Figure 4.6 or Table 4.2, the one with a launch velocity of 10.0 [m/s] and launch azimuth of 45.0 [deg] results in a re-impact scenario when Solar perturbations are omitted but the same initial conditions lead to a temporary capture orbit when perturbations were added for an initial Solar phase angle of 315.0 [deg]. Every other initial condition for the capture cases had otherwise resulted in an escape situation when simulations were conducted without the Solar perturbations. The 3D trajectory plot in two different views for the former case are shown in Figure 4.7 (see Figure A.2 also for the 3D trajectory representation in body fixed frame). The 2D trajectory for the same is shown in Figure 4.8 in inertial frame and in Figure A.3 in the asteroid centric rotating frame or the body frame. The web-link or URL for the trajectory animation of the particle (in inertial frame and in XY plane only) can be found in Figure 4.5.

Figure 4.5: 2D trajectory animation (XY Plane) of capture regolith for case number 5 in Table 4.2. Particle code LoGSP-1. Scan the QR code to view the animation or use the following web-link: `https://youtu.be/oZDhDo5CIsk`
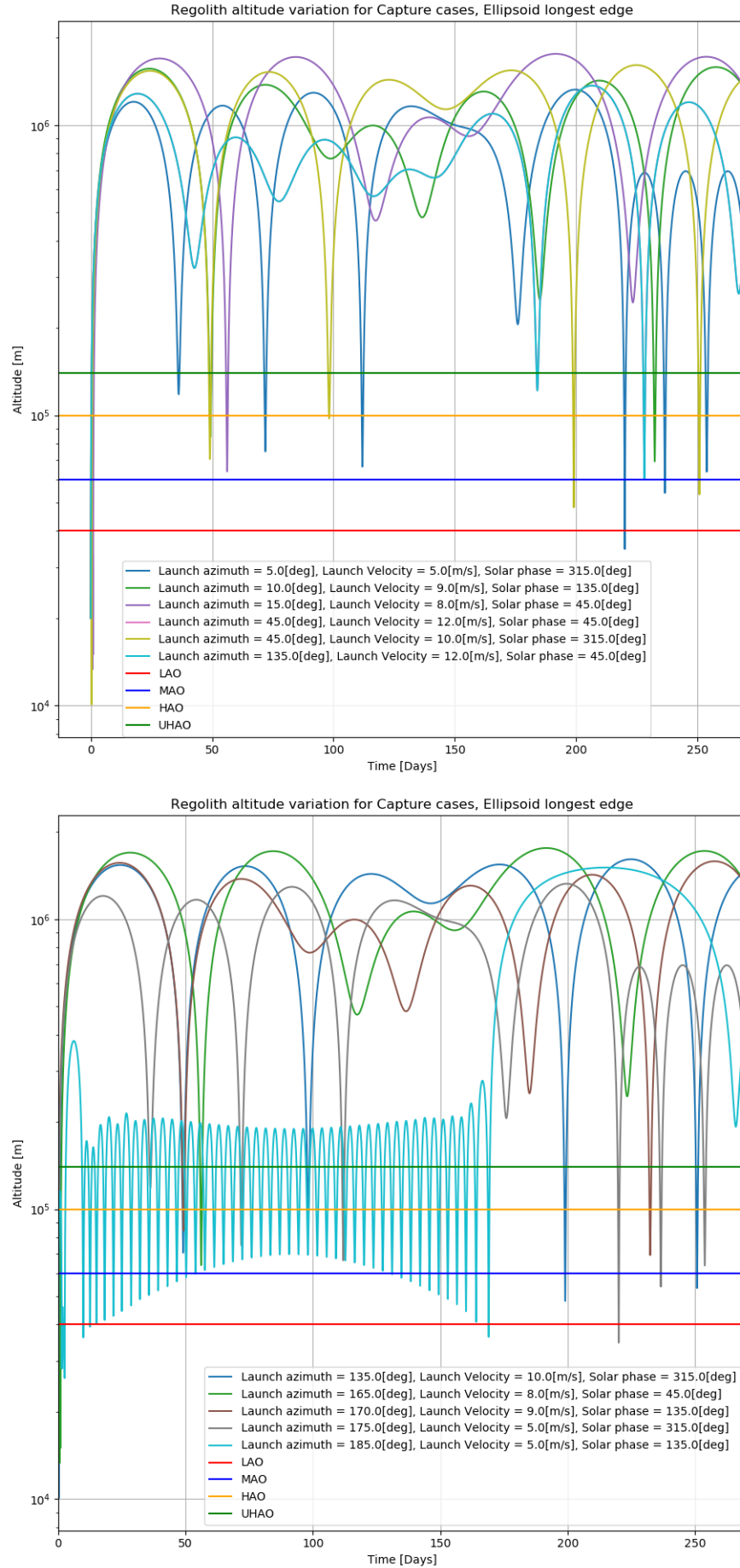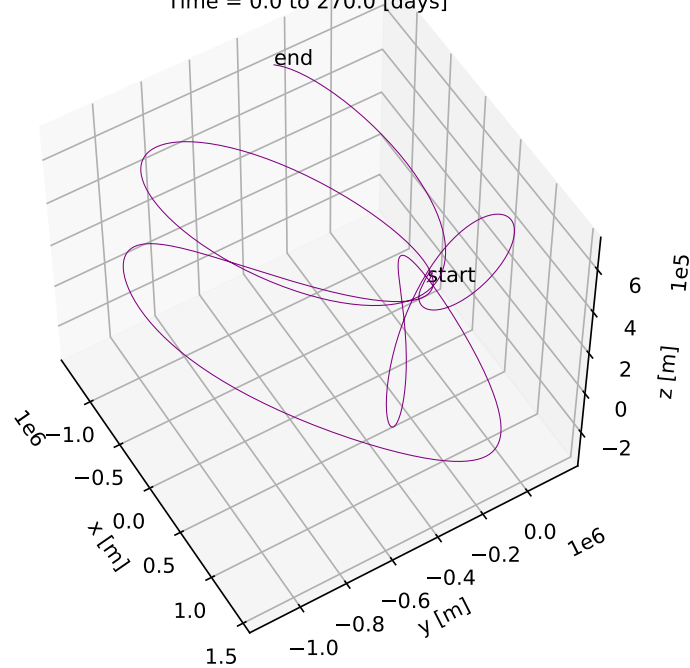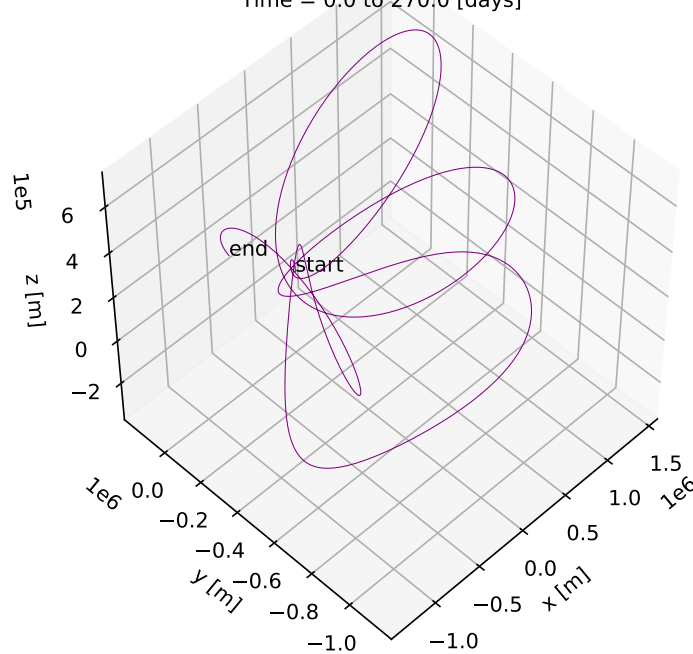
Figure 4.6: Orbital range progression with time for temporary capture scenarios. Particle code LoGSP-1.

(a)

(b)

Figure 4.7: 3D inertial frame trajectory of capture regolith for case number 5 in Table 4.2 in two different viewing angles. Particle code LoGSP-1.

Note that in the trajectory animation in Figure 4.5 (and any other animation included hence-forth) the particle is made to skip several data points in between along the trajectory when it is far away from the asteroid, just to reduce the length of the animation. So because of this, the particle appears to be moving faster when it is away from the asteroid but this is not true. For the exact veloc-ity of the particle, the reader should look at the velocity magnitude indicator within the animation itself.

The animation shows that the particle reverses its direction of motion twice in its entire course. To visualize how this is happening in 3D, look at Figure 4.7. The reason for this can be understood by looking at the direction of the perturbing acceleration, the gravitational acceleration vectors, and the combined effect of all accelerations acting on the particle. The direction of SRP and STBE are shown in Figure 4.9 and that of the net effect of the two is shown in Figure 4.10a. In the trajec-tory simulator, the gravity model (triaxial ellipsoid model) computes the acceleration in the rotat-ing frame. We calculated the direction of the gravitational acceleration in inertial frame in post-simulation analysis assuming a point-mass model by considering the fact that when the regolith is far-away from the asteroid, its gravity field would appear as that of a point-mass gravity source. The gravitational acceleration vectors are shown in Figure 4.10b. The net acceleration acting on the particle is then shown in Figure 4.11. All acceleration vectors are shown along those parts of the trajectory where the magnitude of SRP acceleration is of the same order of magnitude as that of the gravitational acceleration. However, the magnitude of the STBE acceleration is always 1.0 order of magnitude smaller than the gravitational acceleration for those very same points along the trajec-tory, but is still significant. We do not show the vectors for the entire trajectory for two reasons; first, when close to the asteroid the direction of these vectors would reduce the clarity of the plot and, second, we want to discuss the effect of the perturbations when the particle is far away from the asteroid because then they are as significant as the gravitational force.

In Figure 4.8, the trajectory loops numbered 1 and 2 (XY plane), is where the particle's direction of motion gets reversed. If we look at Figure 4.9a, we see that the direction of the SRP vector is con-sistent with how the particle changes its direction of motion. This, however, does not mean that the SRP is the sole actor responsible for how the particle's motion eventually turns out to be (and we will see this in detail shortly). The direction of STBE, as shown in Figure 4.9b, however, does not directly tell us on how the particle's motion would change as it progresses through its trajectory. STBE is always an order of magnitude smaller than SRP for the points shown in the two plots and its direc-tion is not consistent with how the particle changes its direction of motion but its contribution to the capture scenario is significant (we will see the effect of removing STBE shortly). The direction of the net perturbing acceleration, shown in Figure 4.10a, shows us exactly how and where the motion of the particle is directed. Especially when we look at trajectory loops 1 and 2 in Figure 4.8, we can see that the net perturbing vector is acting in the direction that is consistent with how the particle changes its orbital motion. Now looking at these plots that we just discussed, a question that arises is that - why did the particle remain in a temporary capture orbit, and for example not escape es-pecially when the net perturbing acceleration was acting opposite to the direction of asteroid such as in trajectory loop number 3 in Figure 4.8? The answer to this is found by looking at the direction of gravitational attraction in Figure 4.10b and the total acceleration (i.e. the net effect of gravity and perturbations) acting on the particle in Figure 4.11. Although the gravitational acceleration has the same order of magnitude as that of the Solar perturbations when the particle is far away from the asteroid, we see that the net effect of the two is towards the asteroid and hence prevents the particle from escaping.
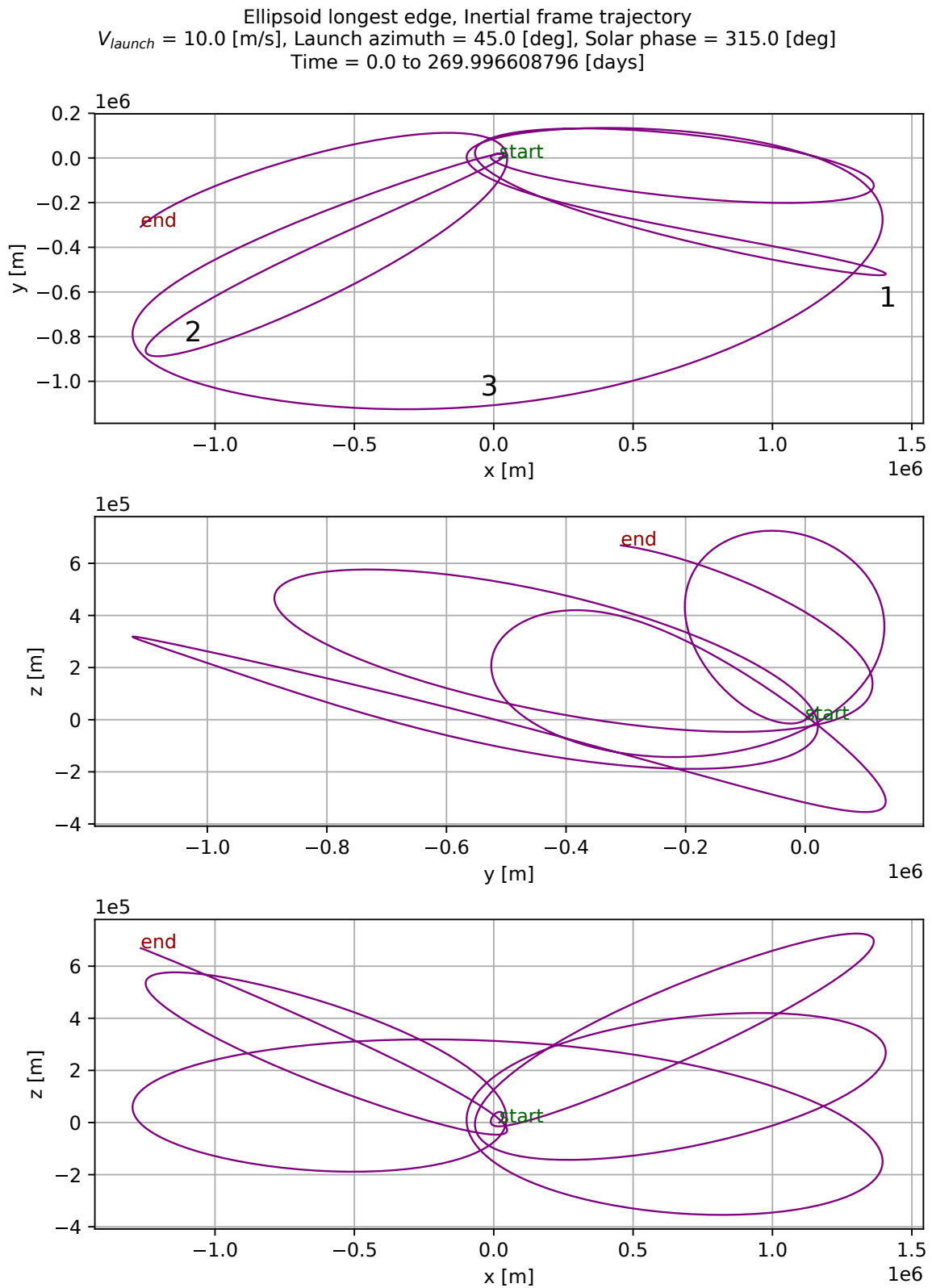
Figure 4.8: 2D inertial frame trajectory of capture regolith for case number 5 in Table 4.2. Particle code LoGSP-1.
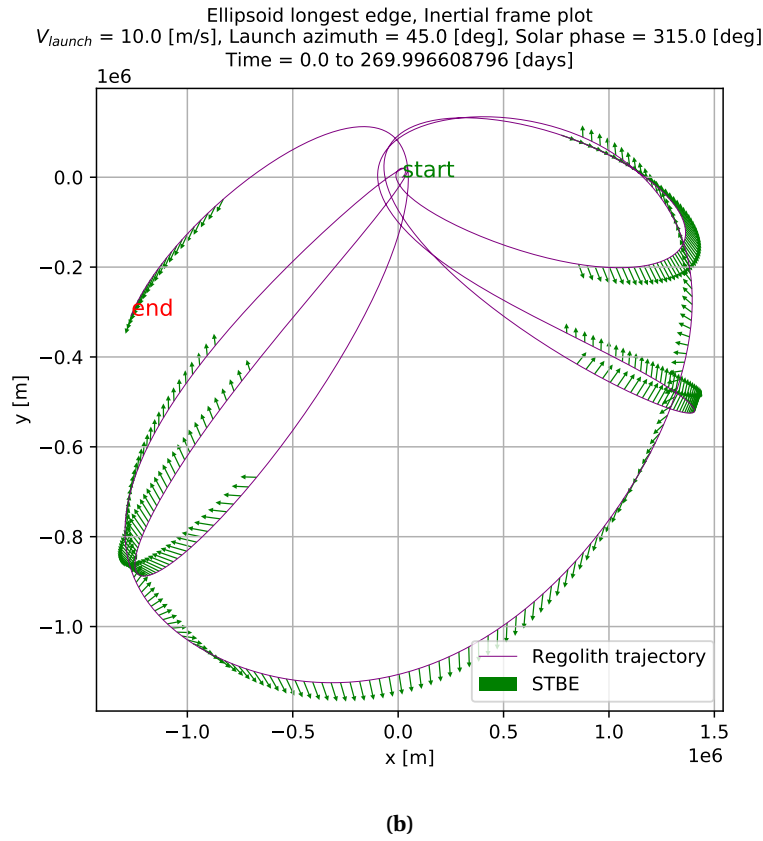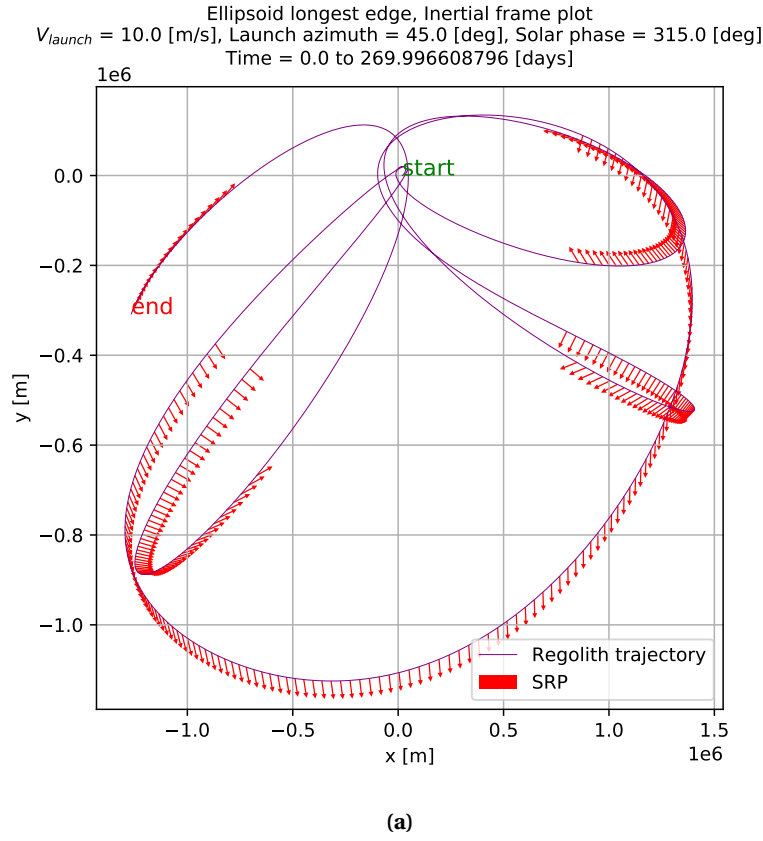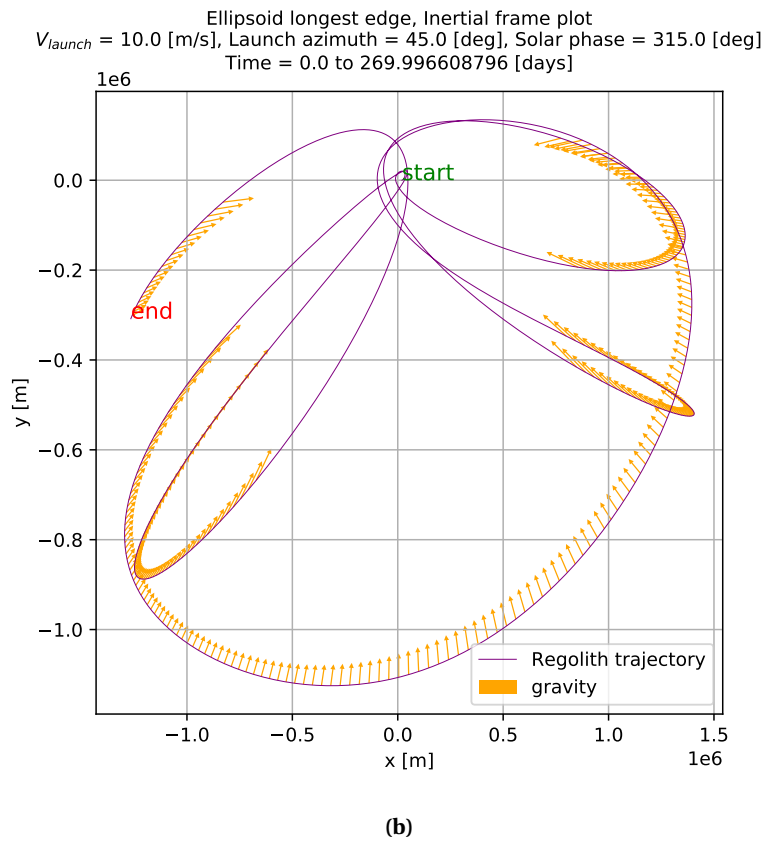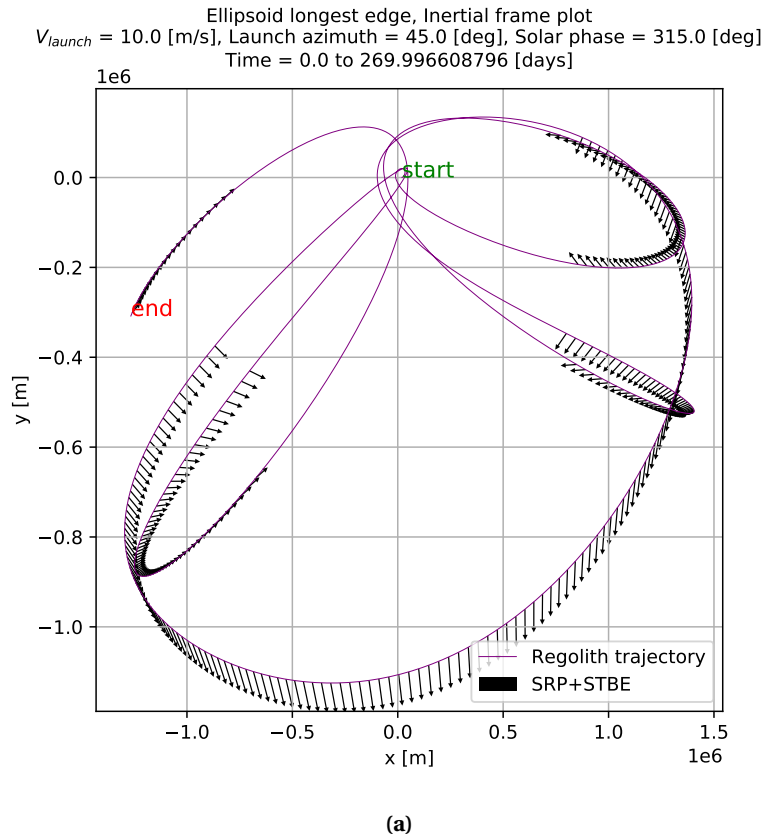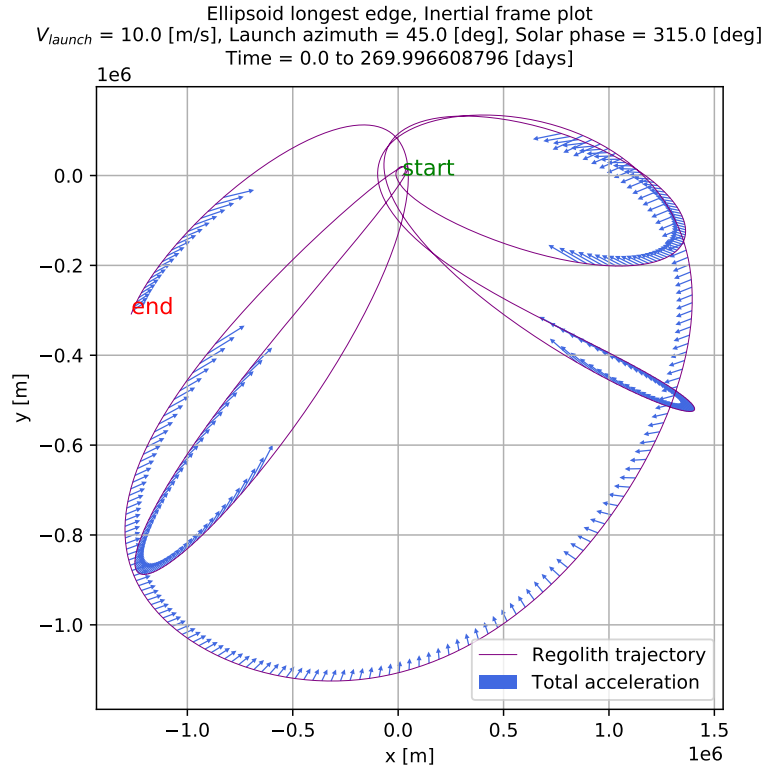
(a)

(b)

Figure 4.9: 2D trajectory of capture regolith for case number 5 in Table 4.2 with direction of SRP and STBE perturbation vectors. Note that the vectors are shown only for those parts of the trajectory where the SRP magnitude is of the same order as that of the asteroid's gravitational acceleration. For those very same points along the trajectory, the magnitude of the STBE is always 1.0 order of magnitude smaller than the gravitational acceleration. Particle code LoGSP-1.

(a)

(b)

Figure 4.10: 2D trajectory of capture regolith for case number 5 in Table 4.2 with direction of the sum total of SRP and STBE perturbation vectors, and the direction of the gravitational acceleration vector for the same data points. Note that the vectors are shown only for those parts of the trajectory where the SRP magnitude is of the same order as that of the asteroid's gravitational acceleration. For those very same points along the trajectory, the magnitude of the STBE is always 1.0 order of magnitude smaller than the gravitational acceleration. Particle code LoGSP-1.

Figure 4.11: 2D trajectory of capture regolith for case number 5 in Table 4.2 with direction of the net acceleration vector. Note that the vectors are shown only for those parts of the trajectory where the SRP magnitude is of the same order as that of the asteroid's gravitational acceleration. For those very same points along the trajectory, the magnitude of the STBE is always 1.0 order of magnitude smaller than the gravitational acceleration. Particle code LoGSP-1.

Both SRP and STBE together are necessary in getting the capture trajectory shown in Figure 4.8. If either one of them is removed from the simulation, for the same launch conditions and initial Solar phase angle, then the results are completely different and we do not get a capture orbit. Note that the definition of capture orbit in this context implies that the particle stays in an orbit around the asteroid for the complete duration of 270.0 [days], i.e., the maximum time for which the simulation is run.

When only STBE is removed, then we get a trajectory where the particle eventually escapes the asteroid. This is shown in Figure 4.12. The trajectory is completely different from the one in Figure 4.8, even though the only difference between the two simulations is the omittion of STBE perturbation. Figure 4.13a shows the direction of perturbing acceleration due to SRP and the gravitational acceleration for those points along the trajectory where both have the same order of magnitude. The direction for the net acceleration acting on the particle is shown in Figure 4.13b. The trajectory of the particle starts out the same way in both Figure 4.12 and Figure 4.8 however due to the lack of STBE perturbation, the trajectories soon start to differ from each other. Upon comparing Figure 4.11 and Figure 4.13b we can infer that the trajectories differ because the with the lack of STBE the direction of the net acceleration vector differs for the two trajectories which eventually directs how the particle motion would progress. The particle trajectory in Figure 4.12 eventually leads to an escape scenario. Now if we look at Figure 4.13a, towards the end of the trajectory, the direction of the gravitational vector gradually changes and starts to point along the instantaneous tangent to the trajectory, all the while with the SRP vector point away from the asteroid. The net effect of this situation can be seen in Figure 4.13b; we see that the net acceleration vector starts pointing away from the asteroid towards the end segment of the trajectory and thus this is when the particle escapes.
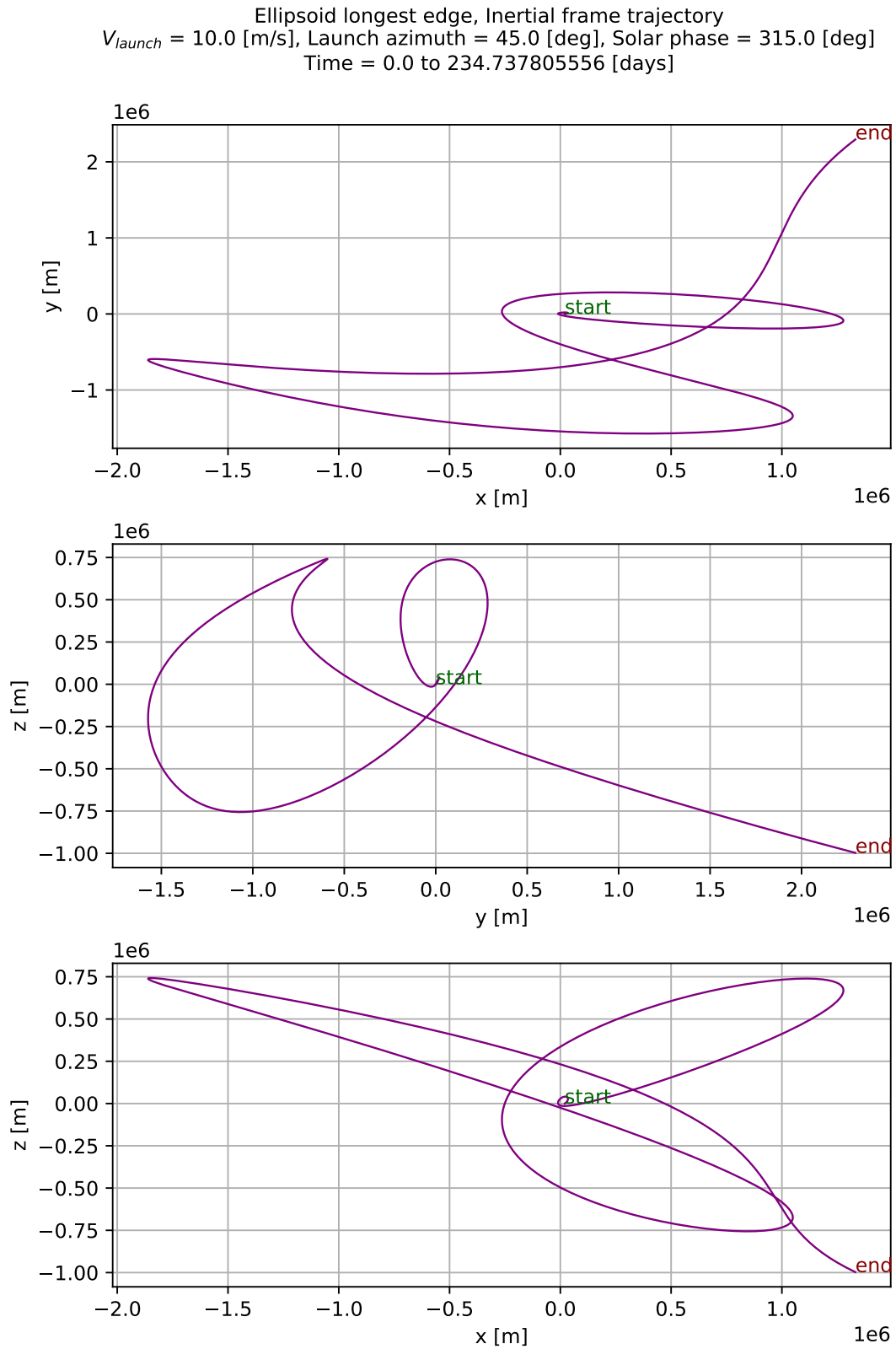
Figure 4.12: 2D trajectory of particle for same initial conditions as that of capture case 5 in Table 4.2 except that only SRP was included in this simulation. Particle code LoGSP-1.
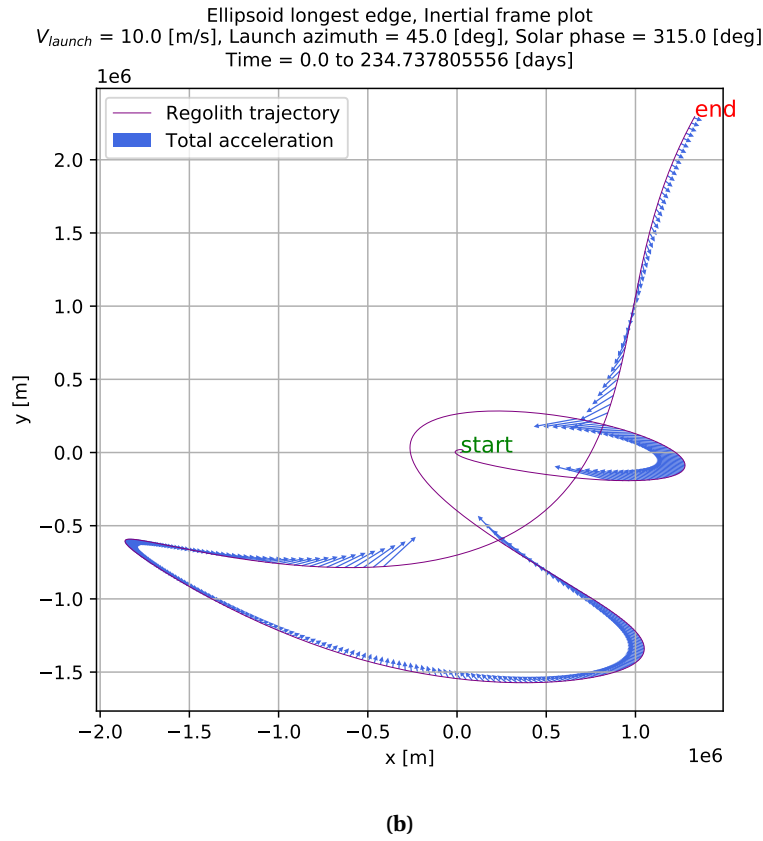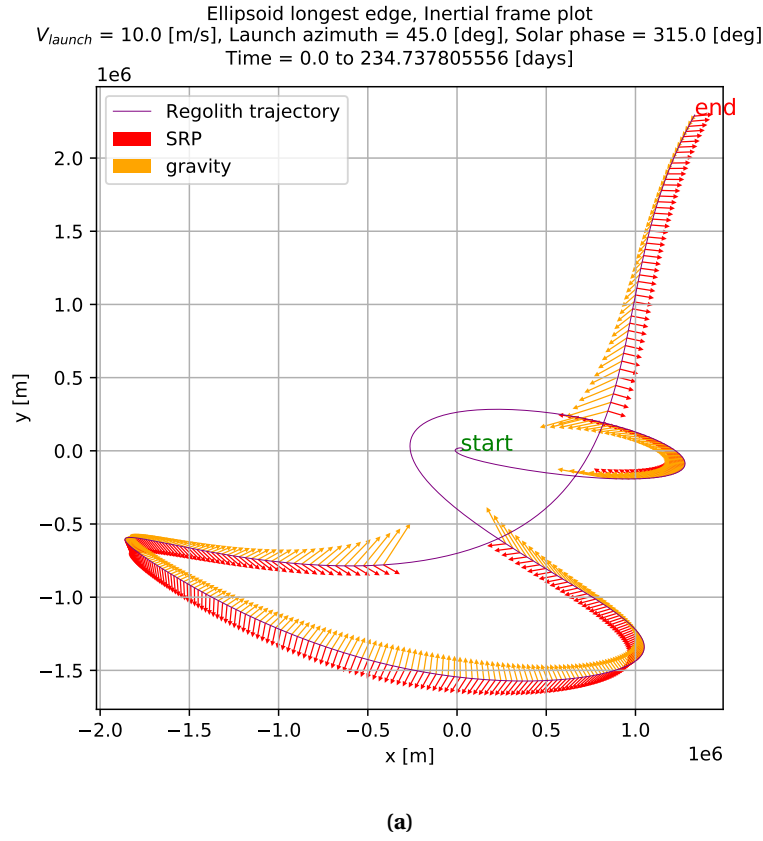
(a)

(b)

Figure 4.13: Inertial frame XY plane trajectory for same launch conditions as that of capture case 5 in Table 4.2: (a) showing direction of SRP acceleration and gravitational acceleration & (b) showing direction of the net acceleration acting on the particle. Vectors are shown only for those parts of trajectory where acceleration due to SRP and gravity have the same order of magnitude. Note that STBE perturbation was not part of the simulation here. Particle code LoGSP-1.

When we keep STBE but remove SRP from our simulations, then the trajectory again leads to an escape situation, only this time its much faster. The 2D inertial frame trajectory is shown in Figure 4.15. The trajectory shows similarity only for a brief moment immediately after launch (notice the small loop after 'start') with the capture case in Figure 4.8 but soon after the particle is on a trajectory that never comes back around the asteroid. The reason for this is clear and simple if one looks at the direction of acceleration due to gravity and STBE in Figure 4.16a and their net effect in Figure 4.16b. Initially, from the point when we show these vectors, we know that the magnitude of STBE acceleration is 1.0 order of magnitude smaller than the gravitational acceleration (see Figure 4.17) and even then the direction of the net acceleration vector is such that the trajectory can not loop around the asteroid. The STBE magnitude increases soon enough to the same order as that of gravitational acceleration and the net acceleration vector direction never points towards the asteroid which eventually causes the particle to escape. However, the point where the magnitude curves of STBE and gravitational acceleration cross is not the point where the escape occurs as is evident from the plot for total energy and eccentricity in Figure 4.14.

From this analysis, we can say that effect of removing SRP from simulations had a much drastic effect than removing just the STBE. Both cases lead to an escape situation and the combined effect of both the perturbations leads to a capture orbit, for the same launch conditions and initial Solar phase angle. The behavior of the trajectory, in all cases, can be easily understood by looking at the direction of the net acceleration vector, especially when the particle is far away from the asteroid because it tells us exactly, how by adding perturbations, the motion of the particle is affected and not just in terms of its final fate but even in terms of changing its orbital direction.
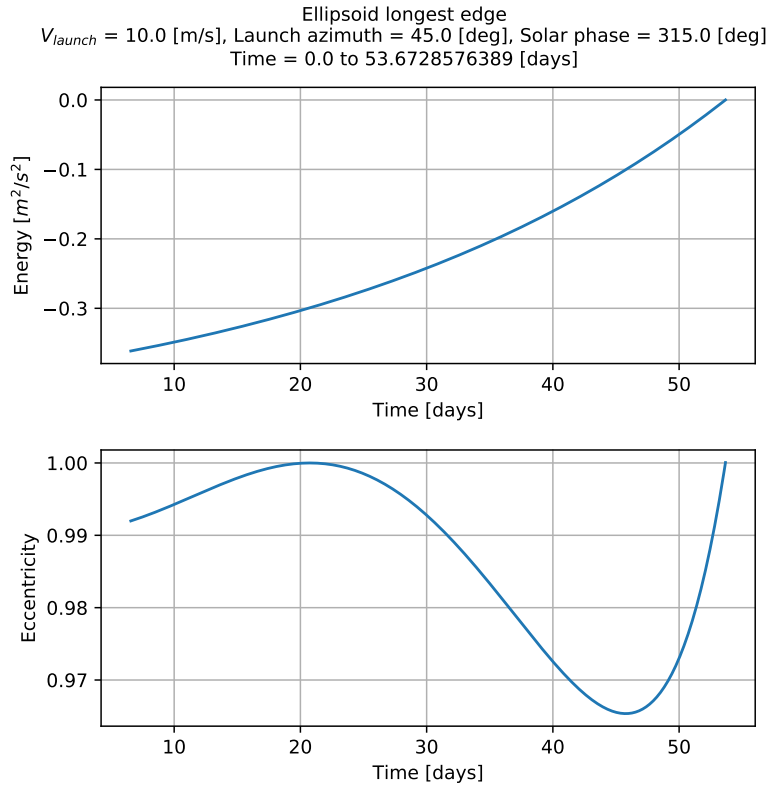

Figure 4.14: Evolution of total energy of the particle and its orbital eccentricity. Particle has the same initial conditions as that of capture case 5 in Table 4.2 except that only STBE was included in this simulation. The range of data points plotted is the same as that in Figure 4.16. Particle code LoGSP-1.
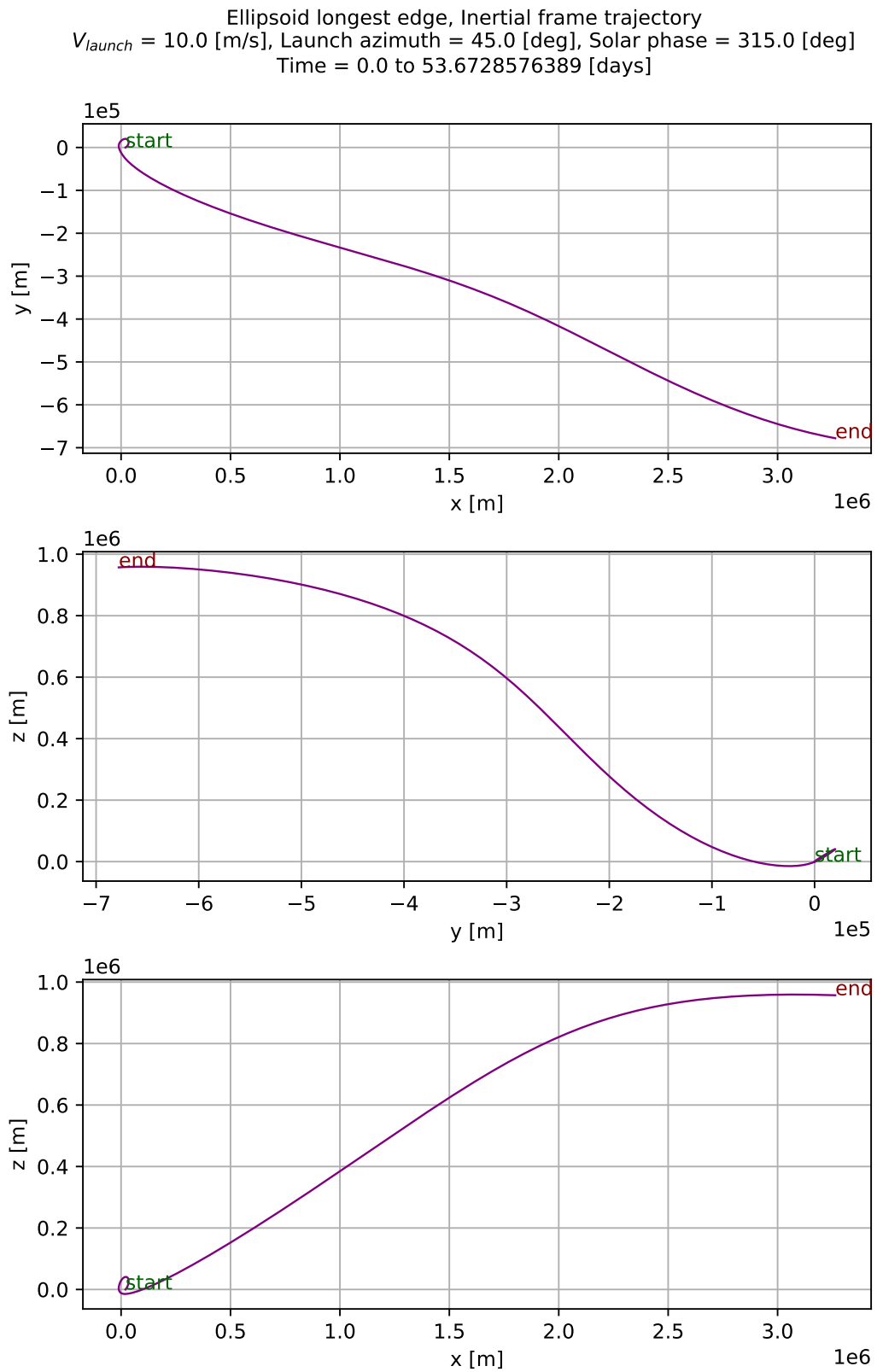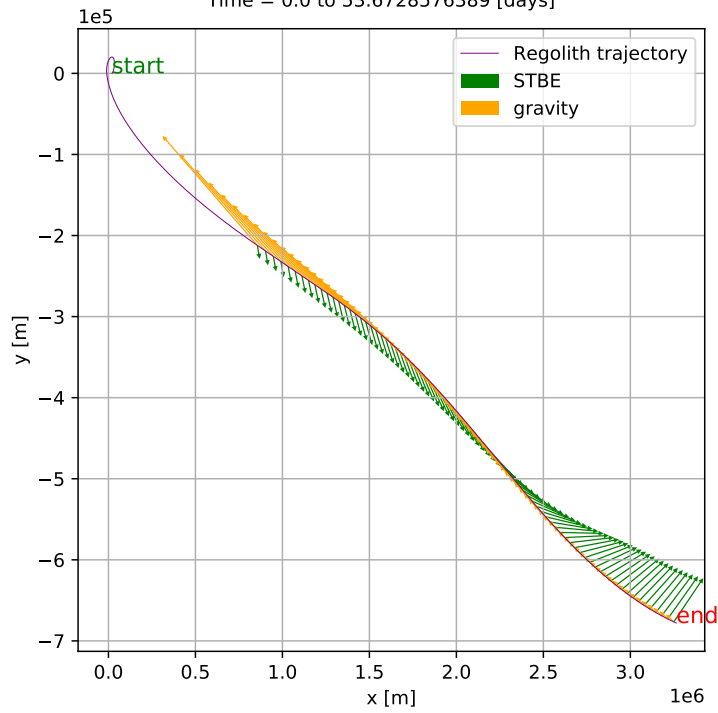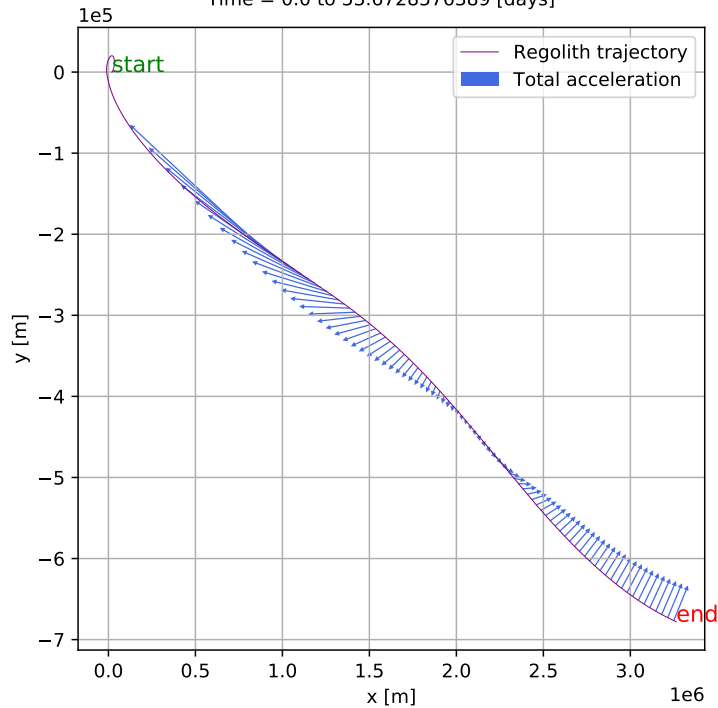
Figure 4.15: 2D trajectory of particle for same initial conditions as that of capture case 5 in Table 4.2 except that only STBE was included in this simulation. Particle code LoGSP-1.

(a)

(b)

Figure 4.16: Inertial frame XY plane trajectory for same launch conditions as that of capture case 5 in Table 4.2: (a) showing direction of STBE acceleration and gravitational acceleration & (b) showing direction of the net acceleration acting on the particle. Vectors are shown only for those parts of trajectory where acceleration due to STBE is equal to gravitational acceleration or smaller than it by 1.0 order of magnitude. Note that SRP perturbation was not part of the simulation here. Particle code LoGSP-1.
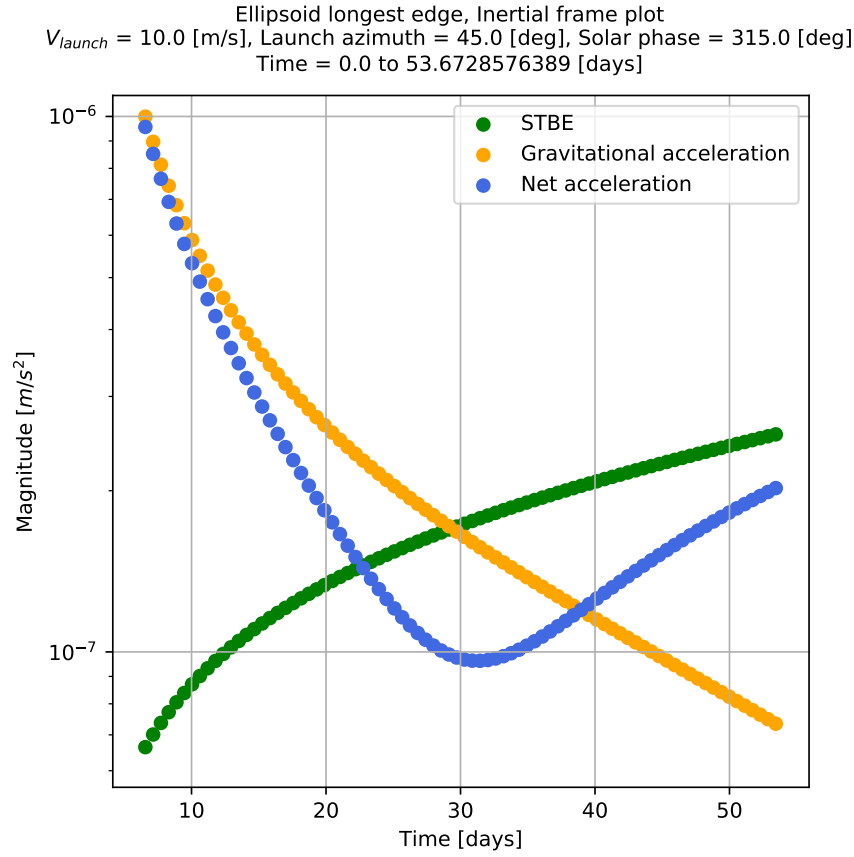
Figure 4.17: Magnitudes of acceleration due to gravity, STBE and the net effect of the two for the corresponding vectors as shown in Figure 4.16. Particle code LoGSP-1.
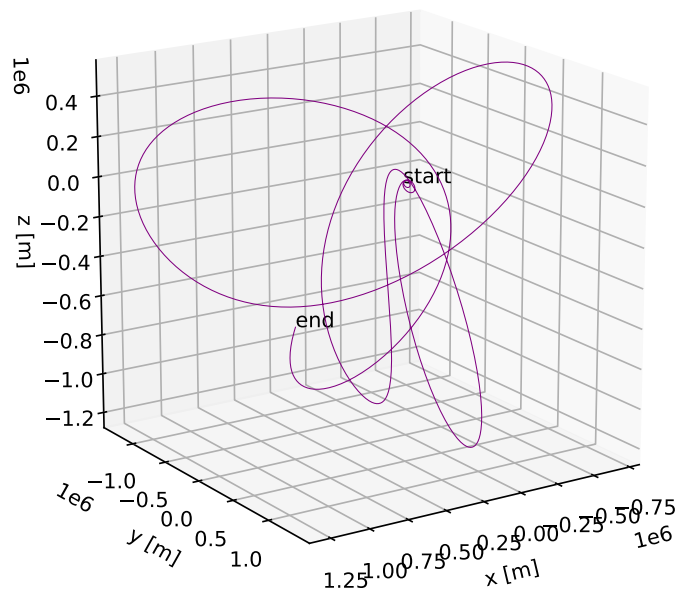
Figure 4.18 shows the 3D trajectory for completely different launch conditions (see capture case 8 in Table 4.2). The 3D trajectory as viewed from the asteroid centric body fixed frame is shown in Figure A.4. The 2D trajectory projections for the same, in inertial and body fixed frames, are shown in Figure 4.19 and Figure A.5 respectively. Just like in the previous case, we see from the animation (see Figure 4.23) and the 3D trajectory for current launch conditions, that the particle direction of motion is reversed twice in its course. These two locations are marked by numbers 1 and 2 in Figure 4.19. At location number 1 we see that the motion changes from anti-clockwise to clockwise direction in the XY plane. The case for location number 2 is exactly the opposite. If we look at Figure 4.21a, the change in direction of motion is consistent with the direction in which the net perturbing force is acting. Ultimately, when we look at the net acceleration acting on the particle in Figure 4.22, we can understand how exactly the particle would orbit around the asteroid. The net force, gravitational and perturbations combined, act in a direction such that the particle is forced to change its orbital motion direction at the two locations previously explained. The acceleration vectors in Figures 4.20 to 4.22 are plotted for points along the trajectory where the magnitude of acceleration due to SRP is of the same order of magnitude as the gravitational acceleration. Again, the magnitude of STBE is 1.0 order of magnitude smaller than the gravitational acceleration for the same data points along the trajectory.

(a)

(b)

Figure 4.18: 3D inertial frame trajectory of capture regolith for case number 8 in Table 4.2 from two different viewing angles. Particle code LoGSP-1.
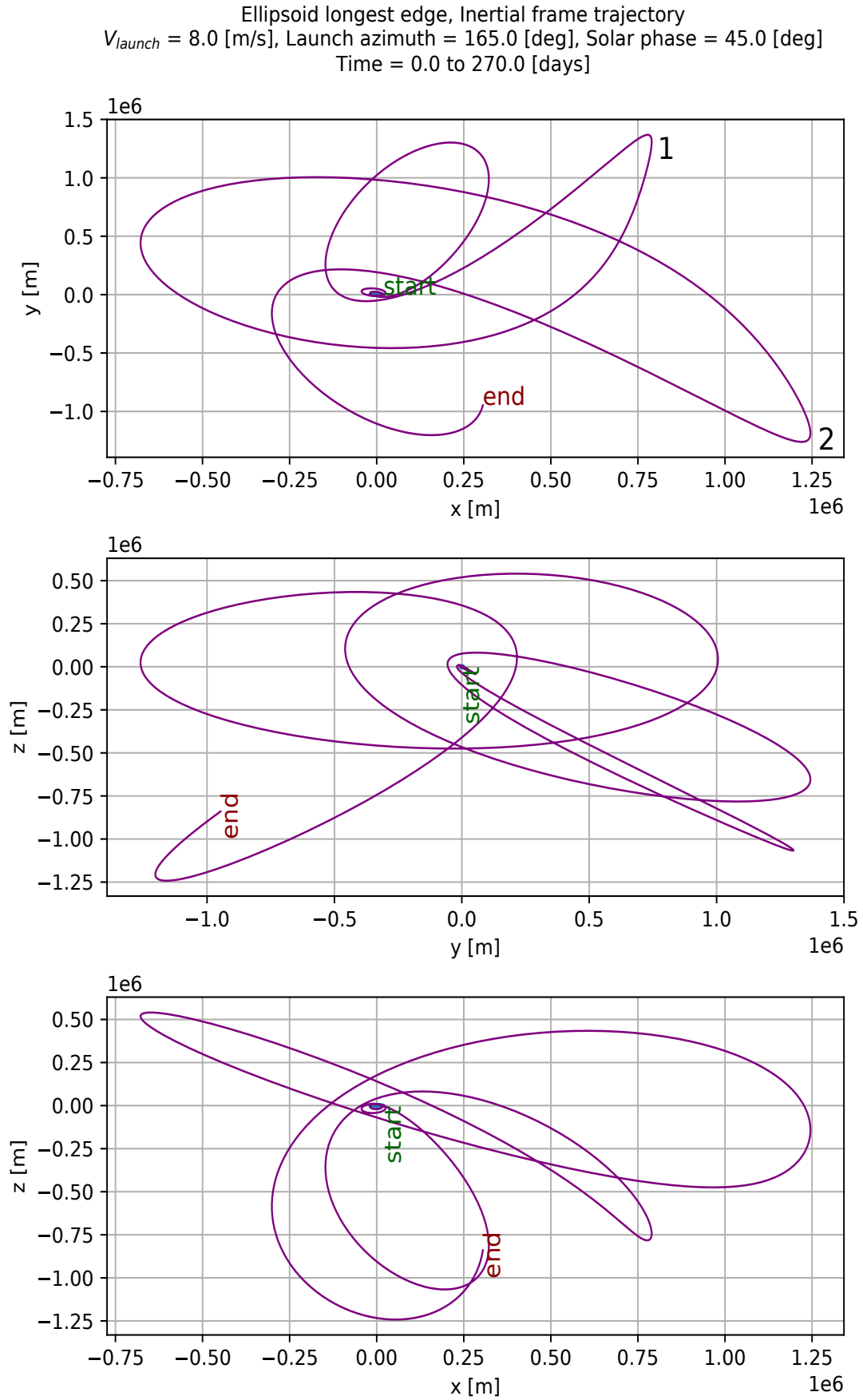
Ellipsoid longest edge, Inertial frame trajectory
V_{launch} = 8.0 [m/s], Launch azimuth = 165.0 [deg], Solar phase = 45.0 [deg]
Time = 0.0 to 270.0 [days]

Figure 4.19: 2D inertial frame trajectory of capture regolith for case number 8 in Table 4.2. Particle code LoGSP-1.
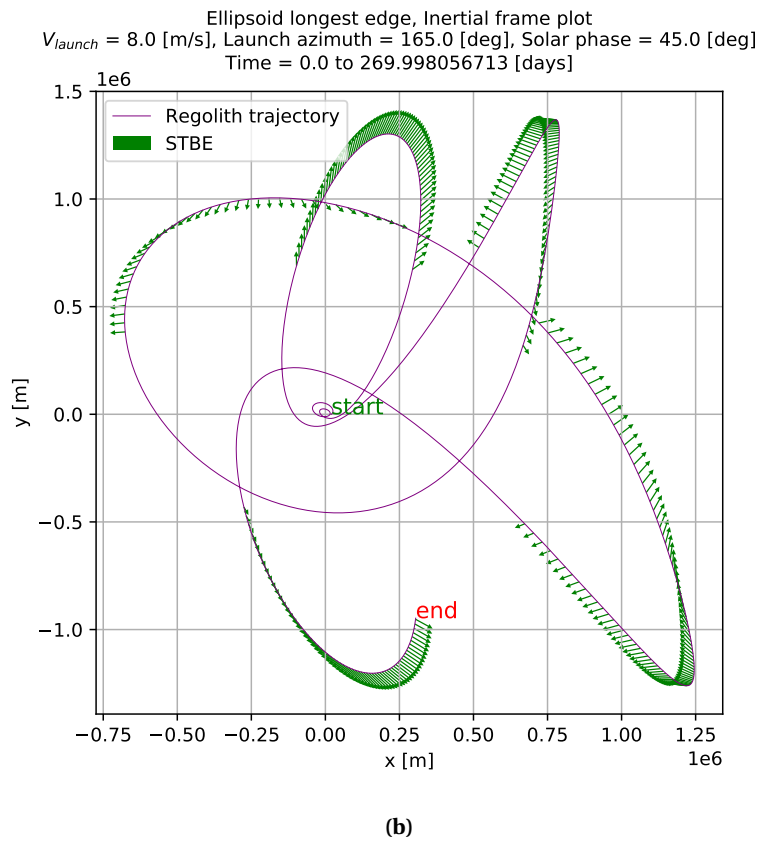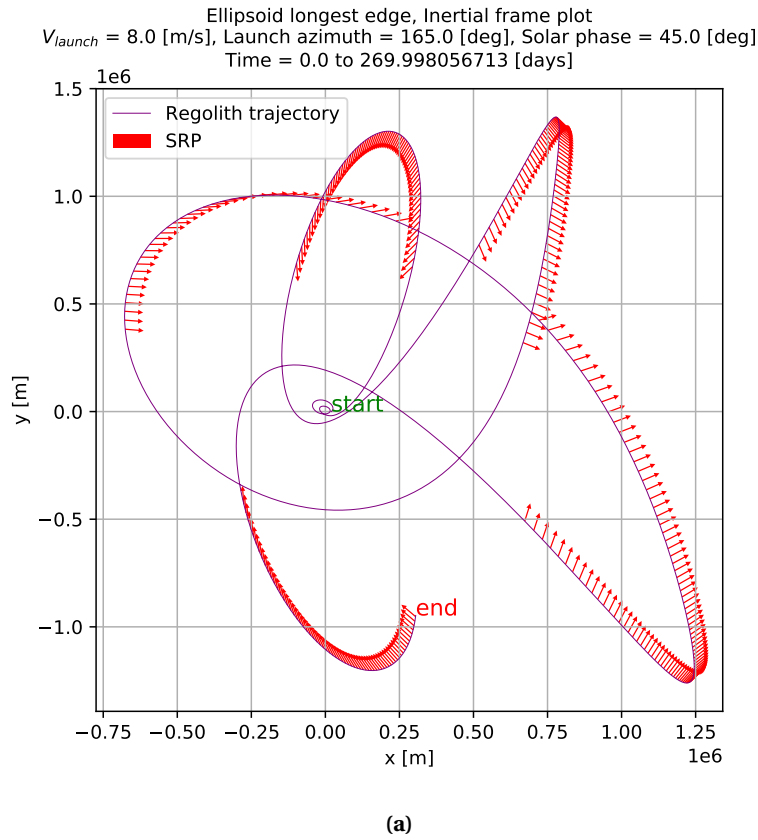
(a)

(b)

Figure 4.20: 2D trajectory of capture regolith for case number 8 in Table 4.2 with direction of SRP and STBE perturbation vectors. Note that the vectors are shown only for those parts of the trajectory where the SRP magnitude is of the same order as that of the asteroid's gravitational acceleration. For those very same points along the trajectory, the magnitude of the STBE is always 1.0 order of magnitude smaller than the gravitational acceleration. Particle code LoGSP-1.
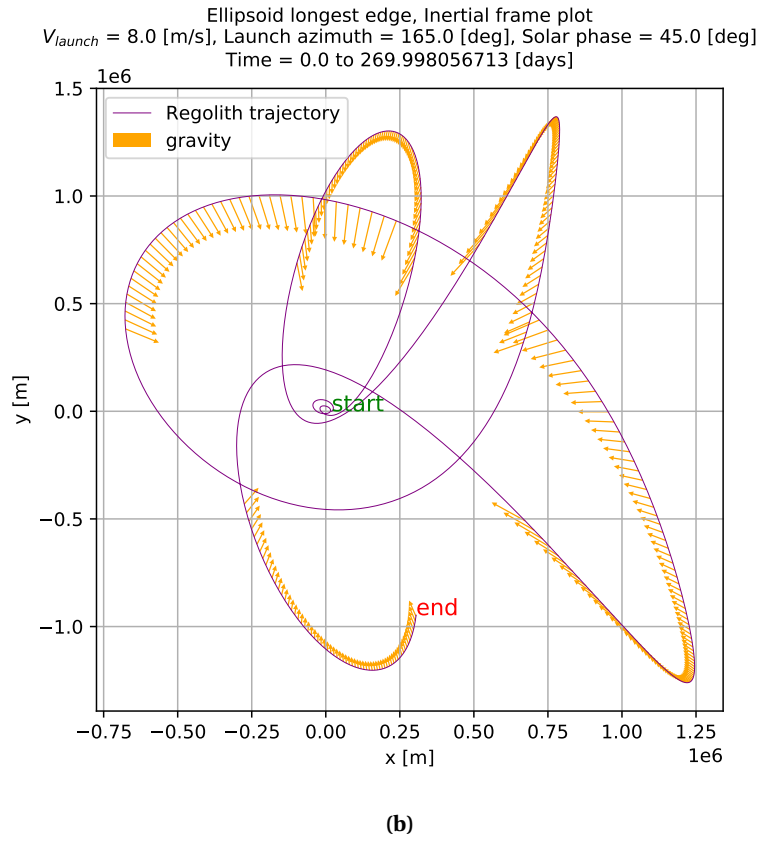
(a)

(b)

Figure 4.21: 2D trajectory of capture regolith for case number 8 in Table 4.2 with direction of the sum total of SRP and STBE perturbation vectors, and the direction of the gravitational acceleration vector for the same data points. Note that the vectors are shown only for those parts of the trajectory where the SRP magnitude is of the same order as that of the asteroid's gravitational acceleration. For those very same points along the trajectory, the magnitude of the STBE is always 1.0 order of magnitude smaller than the gravitational acceleration. Particle code LoGSP-1.
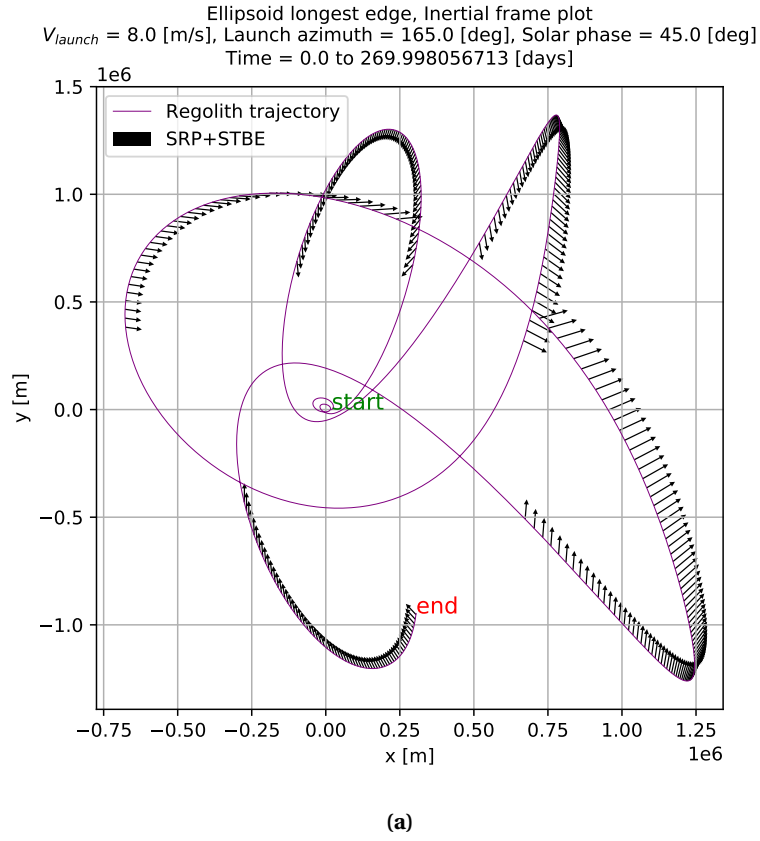
Figure 4.22: 2D trajectory of capture regolith for case number 8 in Table 4.2 with direction of the net acceleration vector. Note that the vectors are shown only for those parts of the trajectory where the SRP magnitude is of the same order as that of the asteroid's gravitational acceleration. For those very same points along the trajectory, the magnitude of the STBE is always 1.0 order of magnitude smaller than the gravitational acceleration. Particle code LoGSP-1.
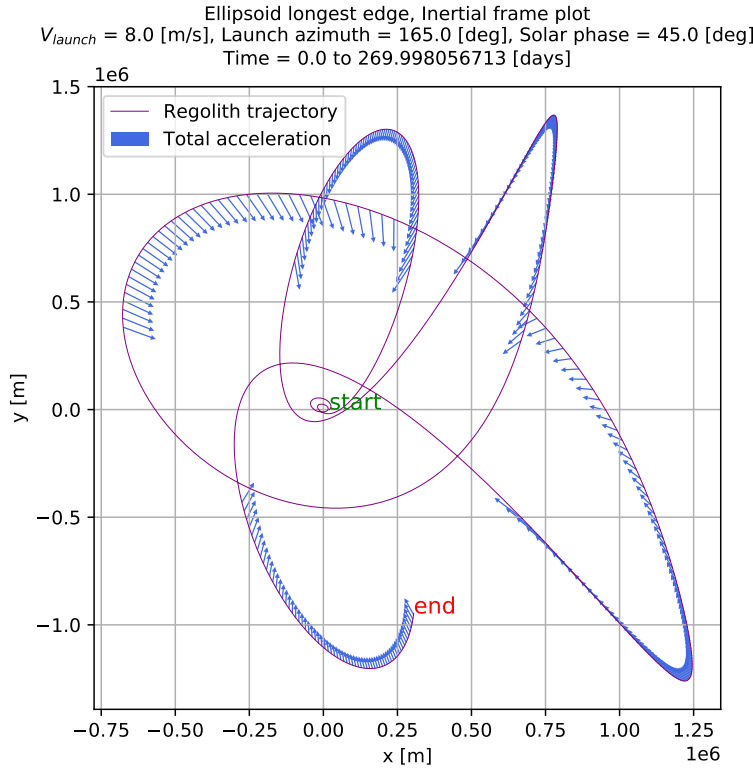

Figure 4.23: 2D trajectory animation (XY Plane) of capture regolith for case number 8 in Table 4.2. Particle code LoGSP-1. Scan the QR code to view the animation or use the following web-link: `https://youtu.be/CceYRlNvAiM`

We saw in the analysis of capture case number 5 for particle LoGSP-1 that both SRP and STBE were necessary for getting that specific capture trajectory and removal of either of the perturbations resulted in a different final fate for the same particle. The next analysis that we present now, will tell us about how a capture scenario occurs, relative to a situation when all perturbations are removed, for the same initial launch conditions in both cases. We do the analysis for capture case number 8 from Table 4.2. Figure 4.25a shows two different trajectories for the particle launched with the same initial conditions. The one shown in dotted line is for the case when Solar perturbations were omitted from the simulation, which eventually results in the particle escaping the asteroid after 1.4 [days]. The one in the solid line shows the capture trajectory (actually a section of the entire capture trajectory as seen in Figure 4.19) when Solar perturbations were included in the simulation. Note that we show the perturbed trajectory (capture case) for the same amount of time (1.4 [days] instead of 270.0 [days]) as taken by the unperturbed trajectory (escape case) to be able to do a one-to-one comparison. The arrows plotted along this trajectory indicate the direction of the net perturbing

acceleration due to SRP and STBE. Figure 4.24 directs to an animation for both the unperturbed and perturbed trajectory.

Figure 4.24: 2D trajectory animation (XY Plane) of capture regolith for case number 8 in Table 4.2, compared with that of its unperturbed counterpart. Particle code LoGSP-1. Scan the QR code to view the animation or use the following web-link: `https://youtu.be/CdFKKR3UDJO`

From the animation we can see that even as the particle has just been lofted from the surface of the asteroid, there are very subtle and minute differences in the range to the particle and its velocity, between the perturbed and unperturbed trajectory. The first visible difference between the two trajectories becomes noticeable at point *"A"* in Figure 4.25a. It is easy to deduce the change in the perturbed trajectory from the direction of the net perturbing acceleration up until this point. The same point *"A"* is also marked in Figure 4.25b. It is from this point that we can see noticeable difference between the two trajectories as well as in their corresponding energies. A snippet from the trajectory animation, corresponding to the point *"A"*, is shown in Figure 4.29a which highlights the differences in range and velocity of the particles in the two trajectories. Note that in Figure 4.29a, the difference in the velocity between the perturbed and unperturbed cases is relatively small, compared to almost 1 [km] of a difference in range of the particles. The latter is significant since the particles have dimensions in the order of [cm]. From point *"A"* onwards these differences continue to grow and only get larger as the trajectory proceeds.

Similarly, at point *"B"* in Figure 4.25a, we see a much larger difference in the two trajectories. In Figure 4.25b, we see that around point *"B"* both trajectories have a positive energy which quickly comes down to a negative value for the perturbed trajectory, hence keeping it bounded which results in a capture scenario. However, this does not happen for the unperturbed trajectory, leading to an escape scenario. The difference in the state of the two particles at point *"B"* are relatively larger and can be seen in Figure 4.29b. The differences in the two trajectories, computed in the asteroid centric rotating frame, is shown in Figure 4.26. The plot on the bottom shows the trajectory for 1.4 [days] (i.e. until escape for the unperturbed trajectory) as viewed in the rotating frame, and the plot on the right zooms into a small part of this trajectory to show how Solar perturbations are responsible for changing the course of the particle. It is seen with a bit more clarity on how the net perturbation vector pulls the trajectory away from the trace of the unperturbed one.

So what we are seeing here is, that due to the inclusion of perturbations from the Sun, the motion of the particle changed from its unperturbed counterpart. This change was not drastic in terms of the initial shape of the trajectory as seen in Figure 4.25a. But the change was just enough for the particle to have a different phase with respect to the asteroid, relative to the unperturbed trajectory as seen in Figure 4.29. By phase, we refer to the location of the particle with respect to a given rotational state of the asteroid. So if two particles are at different locations, at any given epoch and for the same rotational state of the asteroid, they will have different magnitudes of forces acting on them which would ultimately lead to different final outcomes.
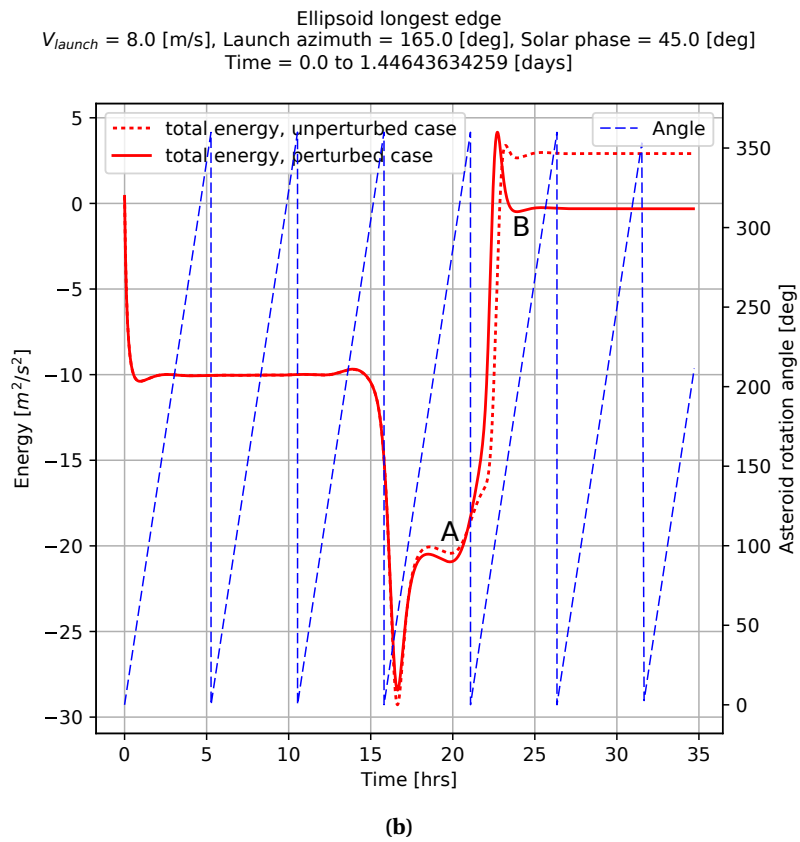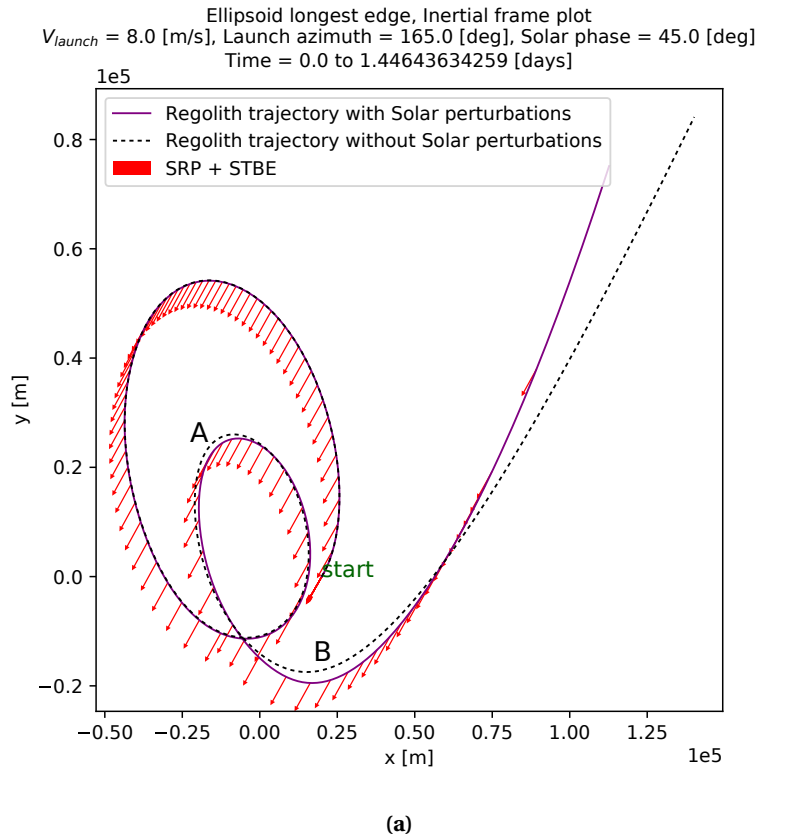
Ellipsoid longest edge, Inertial frame plot
V_{launch} = 8.0 [m/s], Launch azimuth = 165.0 [deg], Solar phase = 45.0 [deg]
Time = 0.0 to 1.44643634259 [days]

(a)

Ellipsoid longest edge
V_{launch} = 8.0 [m/s], Launch azimuth = 165.0 [deg], Solar phase = 45.0 [deg]
Time = 0.0 to 1.44643634259 [days]

(b)

Figure 4.25: Comparative analysis of capture case 8 in Table 4.2 with a particle trajectory where the initial conditions are same as the former but the simulation was done without Solar perturbations. Figure 4.25a compares the XY plane trajectory & Figure 4.25b compares their total energy. Particle code LoGSP-1.
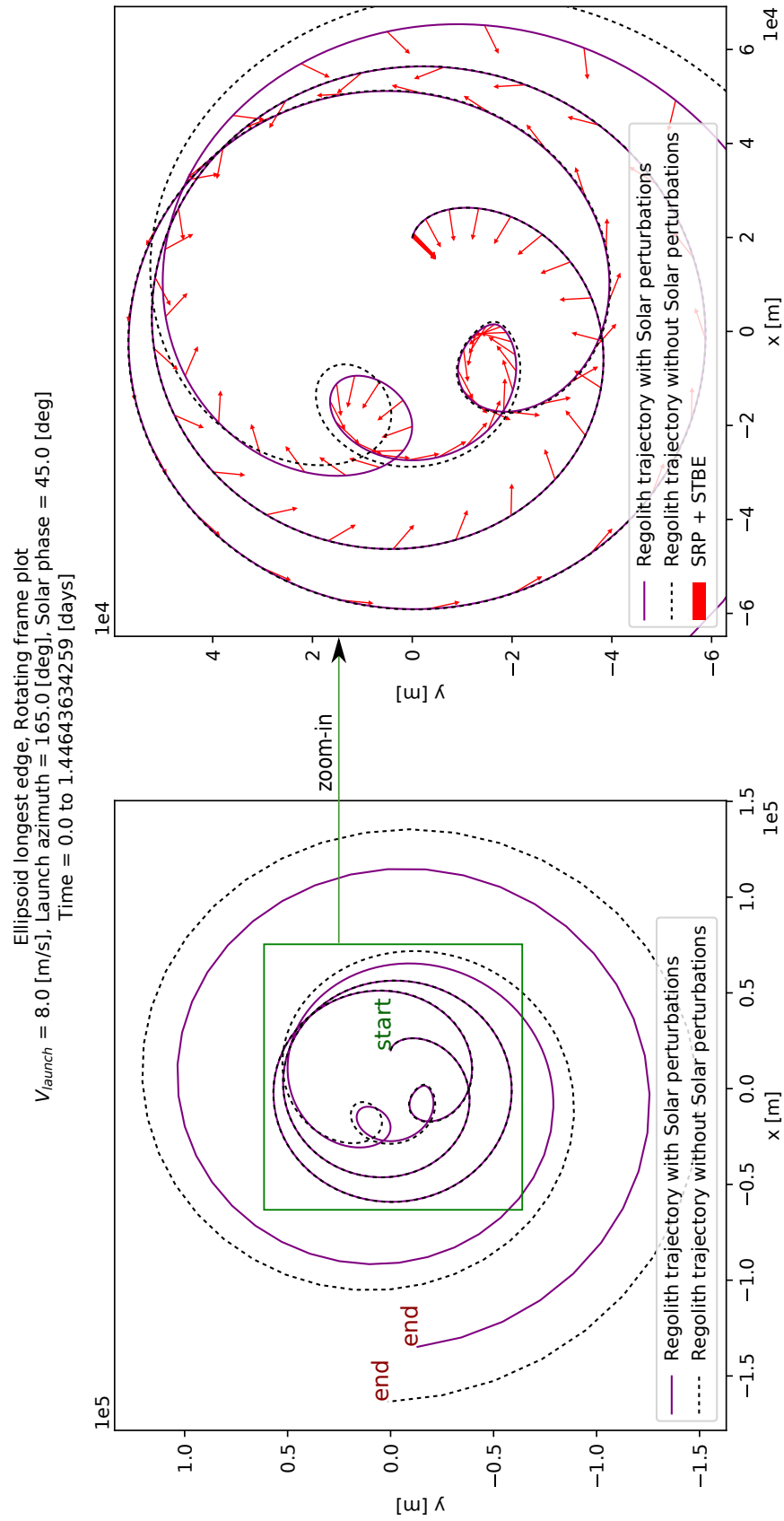
Figure 4.26: Rotating frame 2D trajectory (XY plane) of capture regolith for case number 8 in Table 4.2 with direction of the net perturbation vector, compared with the trajectory of a particle launched with the same initial conditions but in absence of Solar perturbations. Particle code LoGSP-1.
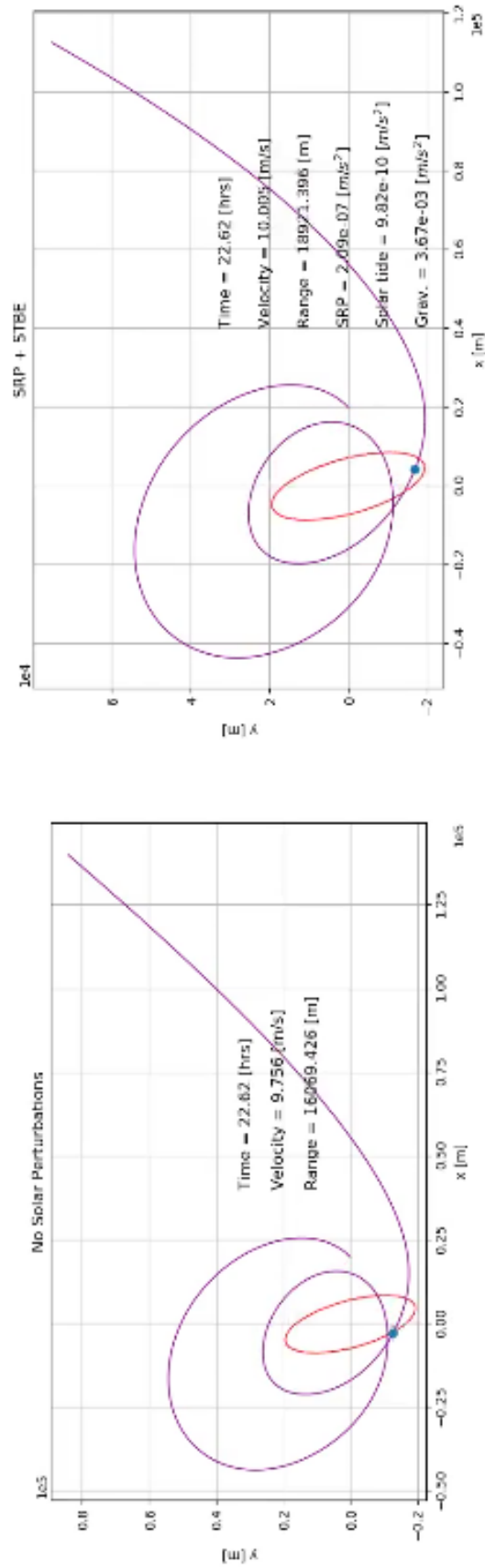
Figure 4.27: Snapshot from animation of the perturbed trajectory of capture case 8 in Table 4.2 compared with that of its unperturbed counterpart. The unperturbed trajectory is still being accelerated at the given instant however the particle in the perturbed trajectory is being decelerated. Particle code LoGSP-1.

If we look at the trajectory animation in Figure 4.24, one would notice that at around point *"B"*, the particle in the unperturbed trajectory is being accelerated by the gravitational pull of the asteroid while the particle in the perturbed trajectory is being slowed down. A snapshot of this scenario from the animation is shown in Figure 4.27. Although this situation does not happen for extended periods of time, but only while approaching point *"B"*, we see that the particle in the unperturbed trajectory has relatively higher velocity while moving forth of point *"B"* and leaving the vicinity of the asteroid, relative to the particle in the perturbed trajectory. The latter thus stays in a capture orbit while the former has enough velocity to escape. A plot for this is shown in Figure 4.28.

Note that in the capture case just discussed, the magnitude of the perturbing accelerations is much smaller than the gravitational acceleration. The effect of the perturbations on the particle's trajectory is not instantaneous and we can see that in the initial part of the trajectories up until point *"A"* in Figure 4.25a. Until this point, acceleration due to gravity is in the order of 10^{-4}, while accelerations due to SRP and STBE are in the orders of 10^{-7} and 10^{-9} respectively. Although the perturbing magnitudes are small, but the particles in question are extremely small as well and so over time, the perturbing accelerations add up, leading to a significant change in the trajectory from the unperturbed one.
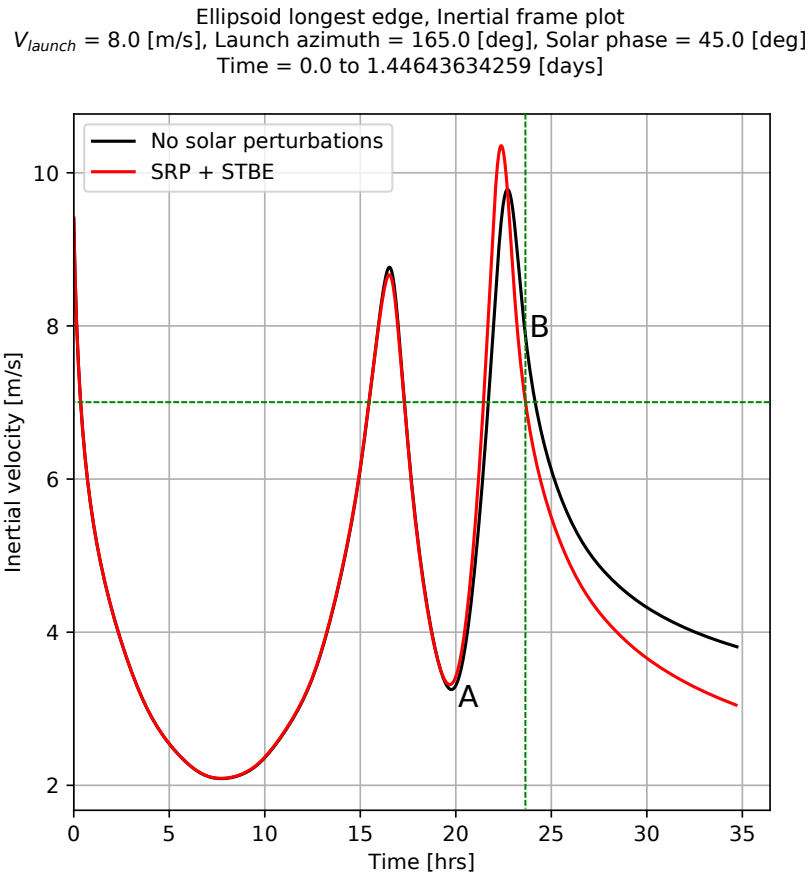

Figure 4.28: Inertial velocity of the perturbed trajectory of capture case 8 in Table 4.2 compared with that of its unperturbed counterpart. The trajectories are shown for the time it takes for the particle in the unperturbed trajectory to escape. Particle code LoGSP-1.
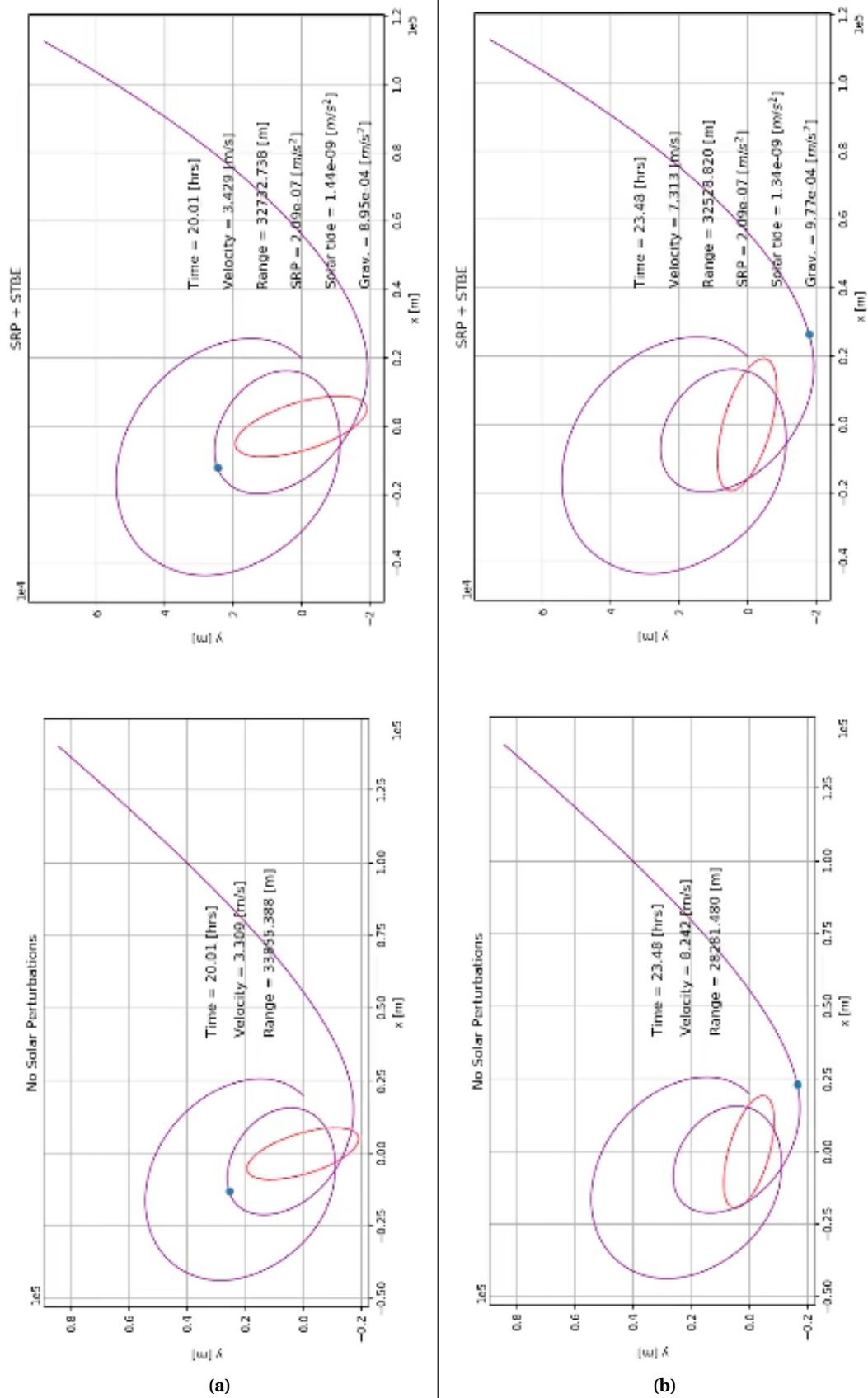
Figure 4.29: Animation snippets of the inertial frame 2D trajectory (XY plane) of capture regolith for case number 8 in Table 4.2. The bottom two plots are for the case when Solar perturbations were omitted from the simulation and the top two plots includes them. Note the differences in the range to the particle and its velocity for the same time stamp and rotational state of the asteroid. Particle code LoGSP-1.

   We see a similar effect when we look at capture case number 5 from Table 4.2. The inertial frame trajectory, both perturbed and unperturbed, for it are shown in Figure 4.30. With Solar perturbations removed from the simulation, the initial conditions for this particle result in it getting launched on a highly elliptical orbit and eventually crashing onto the surface of the asteroid after 96 days. The particle, however, avoids this fate when Solar perturbations are included in the simulation. In Figure 4.30, it can be clearly seen that the direction of the perturbing acceleration due to SRP and STBE is consistent with how the trajectory departs from its unperturbed counterpart. The trajectories are shown only for the time it takes for the particle in the unperturbed trajectory to re-impact the surface of the asteroid. We show this case to highlight the effect perturbations have on a trajectory destined for re-impact, unlike the escape scenario discussed previously. We see drastic changes in the perturbed trajectory from the unperturbed one because when the particle is far away from the asteroid, the perturbing acceleration magnitude is of the same order as that of the gravitational acceleration.
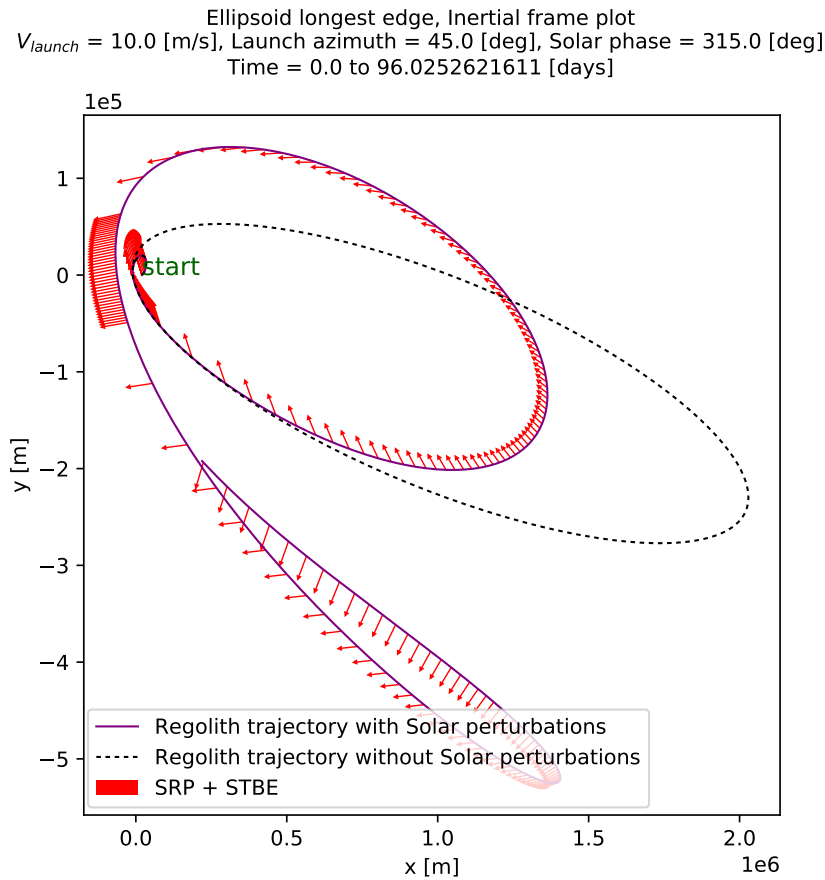

Figure 4.30: Inertial frame 2D trajectory (XY plane) of capture regolith for case number 5 in Table 4.2 with direction of SRP perturbation vector compared with the trajectory of a particle launched with the same initial conditions but in absence of Solar perturbations. Trajectories shown for as long as it takes the unperturbed trajectory Particle code LoGSP-1.

BIBLIOGRAPHY

Evans, Larry G et al. (2001). "Elemental composition from gamma-ray spectroscopy of the NEAR-Shoemaker landing site on 433 Eros". In: *Meteoritics & Planetary Science* 36.12, pp. 1639–1660.

Garcia-Yarnoz, Daniel, Sanchez Cuartielles, Joan-Pau, and McInnes, Colin R (2014). "Passive sorting of asteroid material using solar radiation pressure". In: *Journal of Guidance, Control, and Dynamics* 37.4, pp. 1223–1235.

Jet Propulsion Laboratory, Solar System dynamics, Asteroids. Accessed 1 July 2016. URL: `http://ssd.jpl.nasa.gov/?asteroids`.

Jet Propulsion Laboratory, Why Study Asteroids? Accessed 1 July 2016. URL: `http://ssd.jpl.nasa.gov/?why_asteroids`.

Keller, Lindsay P and Berger, Eve L (2014). "A Transmission Electron Microscope Investigation of Space Weathering Effects in Hayabusa Samples". In:

Marchis, F et al. (2012). "Multiple asteroid systems: Dimensions and thermal properties from Spitzer Space Telescope and ground-based observations". In: *Icarus* 221.2, pp. 1130–1161.

Margot, Jean-Luc et al. (2015). "Asteroid systems: binaries, triples, and pairs". In: *Asteroids IV. University Arizona Press, Tucson*, pp. 355–374.

McCoy, TJ et al. (2001). "The composition of 433 Eros: A mineralogical—chemical synthesis". In: *Meteoritics & Planetary Science* 36.12, pp. 1661–1672.

Nittler, Larry R et al. (2001). "X-ray fluorescence measurements of the surface elemental composition of asteroid 433 Eros". In: *Meteoritics & Planetary Science* 36.12, pp. 1673–1695.

Veverka, J et al. (2001). "Imaging of small-scale features on 433 Eros from NEAR: Evidence for a complex regolith". In: *Science* 292.5516, pp. 484–488.

Appendices

A

EXTRA FIGURES

This appendix contains figures which are used to support the explanation of certain results, arguments and conclusions in the main part of the Thesis report.
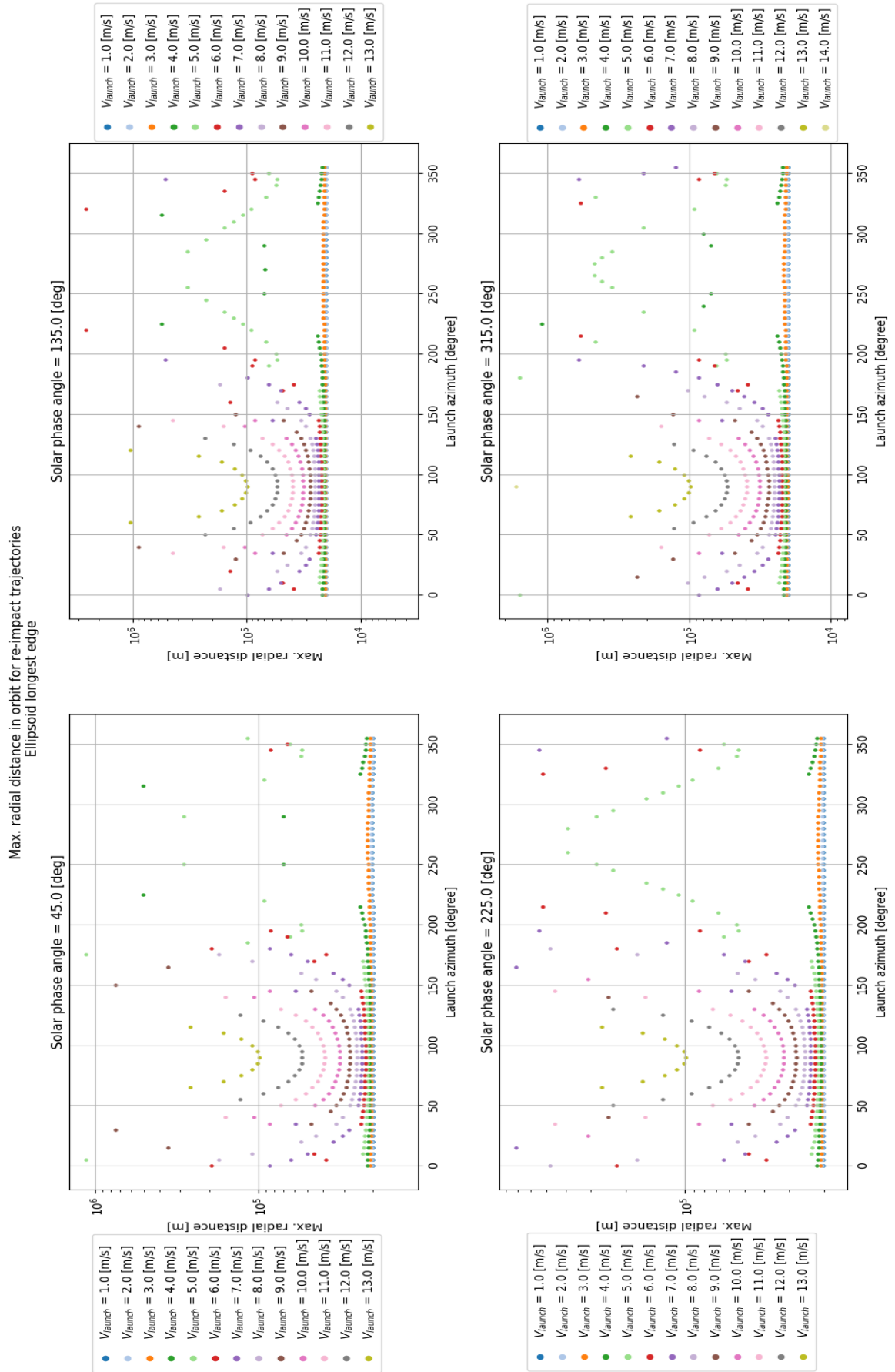
Figure A.1: Maximum radial distance (from the centre of the asteroid) attained by the regolith in orbit for different launch velocities and launch azimuths. The particles were launched from the longest edge of the ellipsoid (asteroid). Plots are for particle code LoGSP-1 and only for the re-impact scenario.
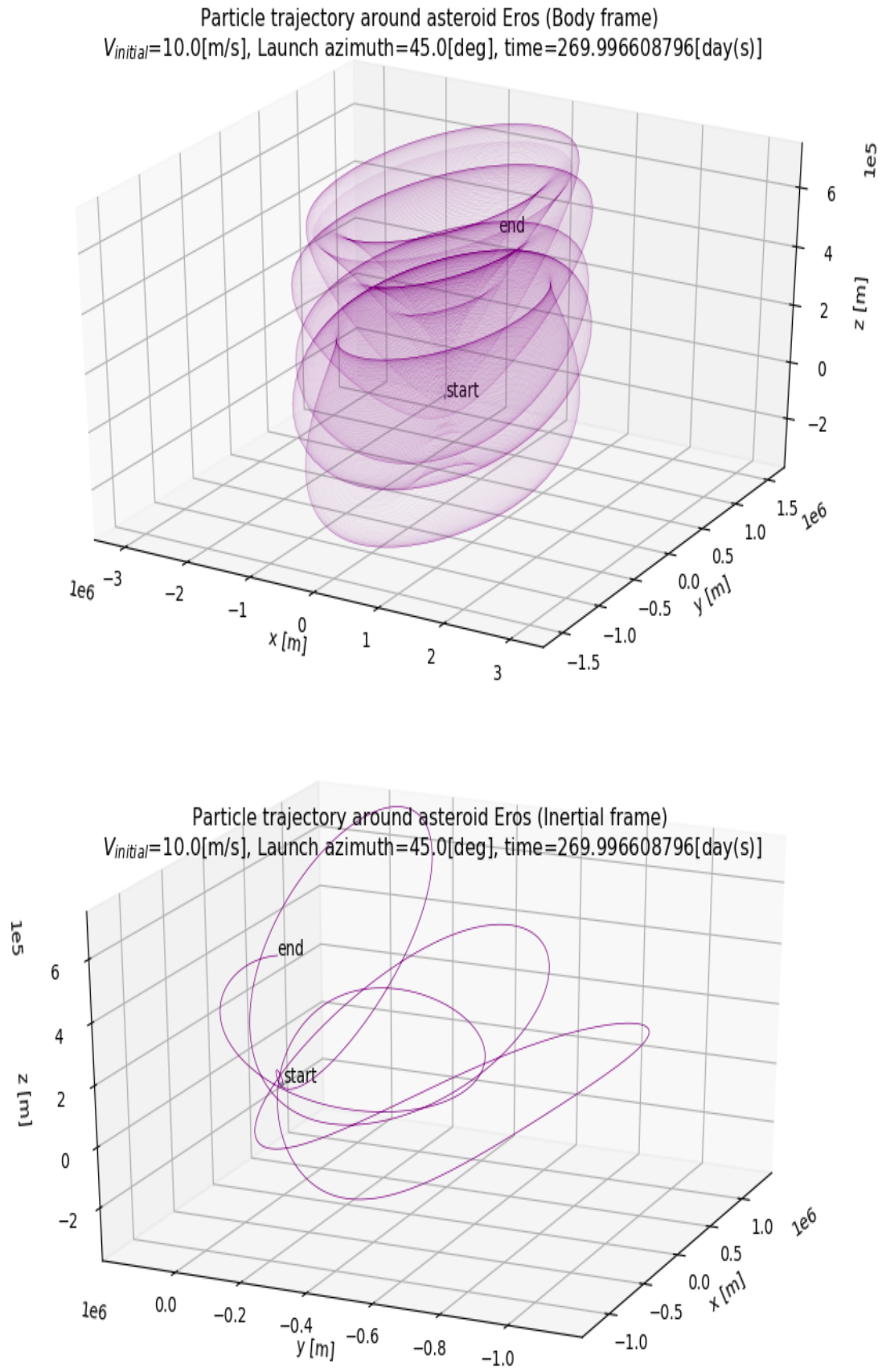
Figure A.2: 3D trajectory of capture regolith for case number 5 in Table 4.2. Particle code LoGSP-1.
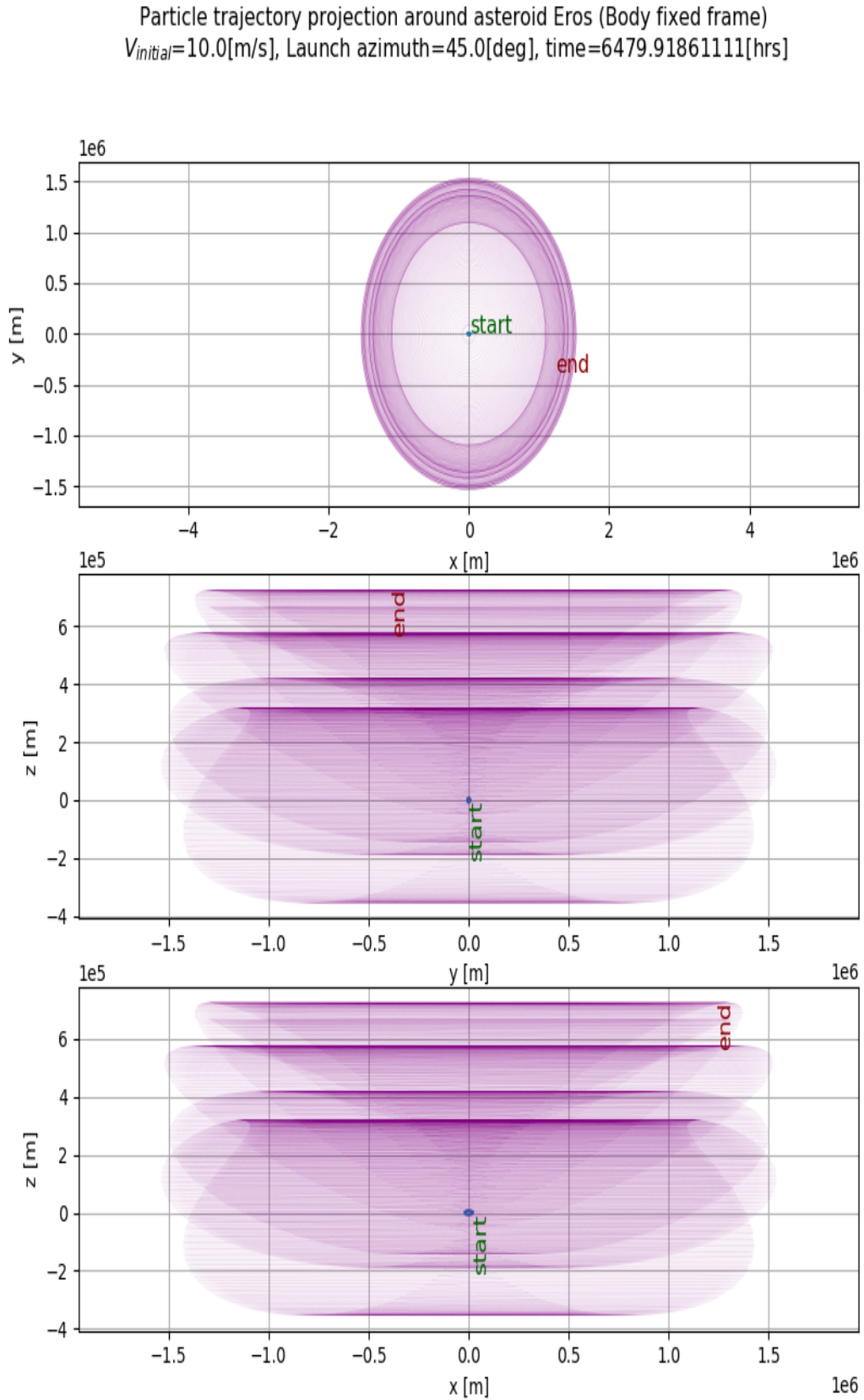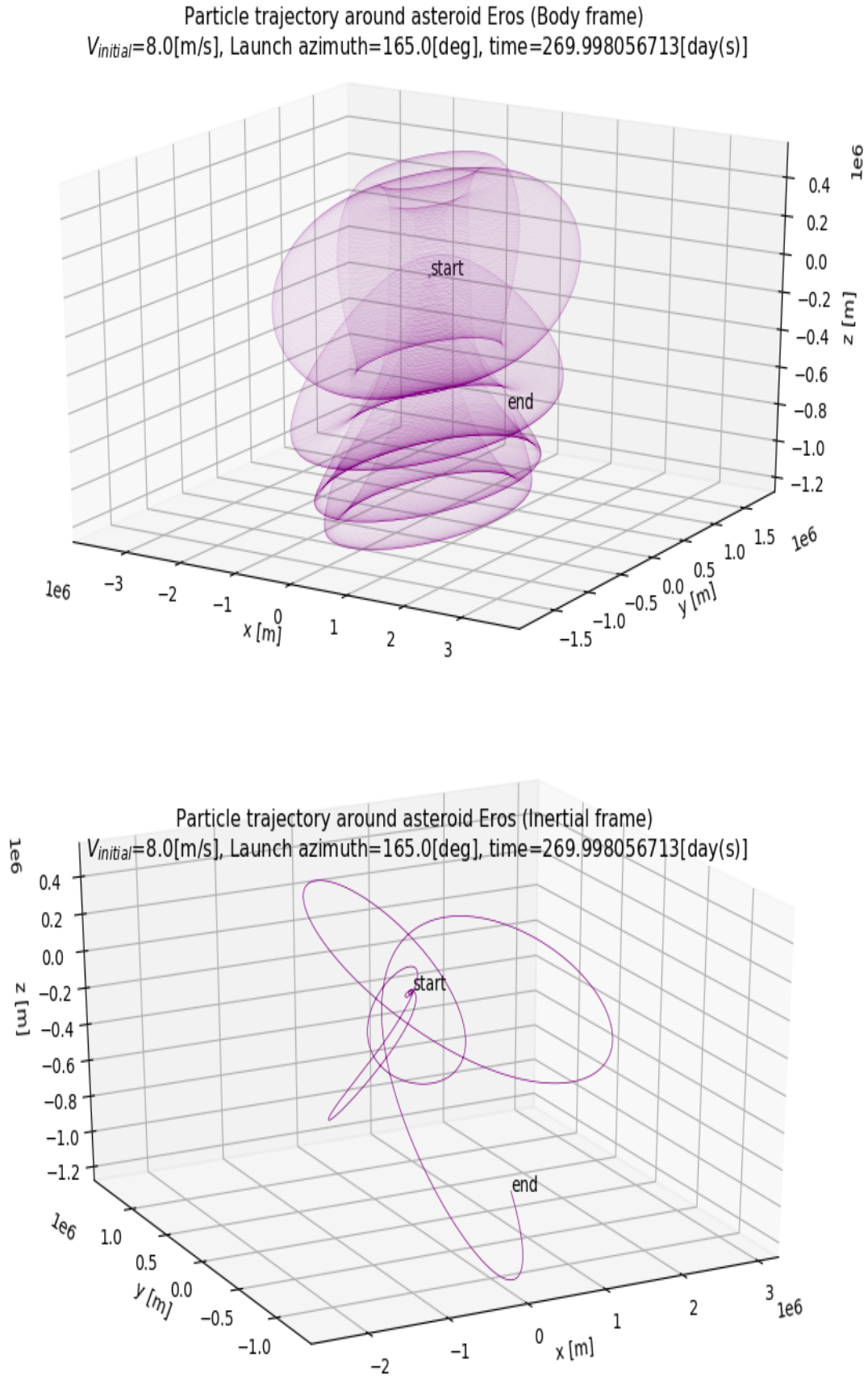
Particle trajectory projection around asteroid Eros (Body fixed frame)
$V_{initial}$=10.0[m/s], Launch azimuth=45.0[deg], time=6479.91861111[hrs]

Figure A.3: 2D rotating frame trajectory of capture regolith for case number 5 in Table 4.2. Particle code LoGSP-1.

Particle trajectory around asteroid Eros (Body frame)
$V_{initial}$=8.0[m/s], Launch azimuth=165.0[deg], time=269.998056713[day(s)]

Particle trajectory around asteroid Eros (Inertial frame)
$V_{initial}$=8.0[m/s], Launch azimuth=165.0[deg], time=269.998056713[day(s)]

Figure A.4: 3D trajectory of capture regolith for case number 5 in Table 4.2. Particle code LoGSP-1.

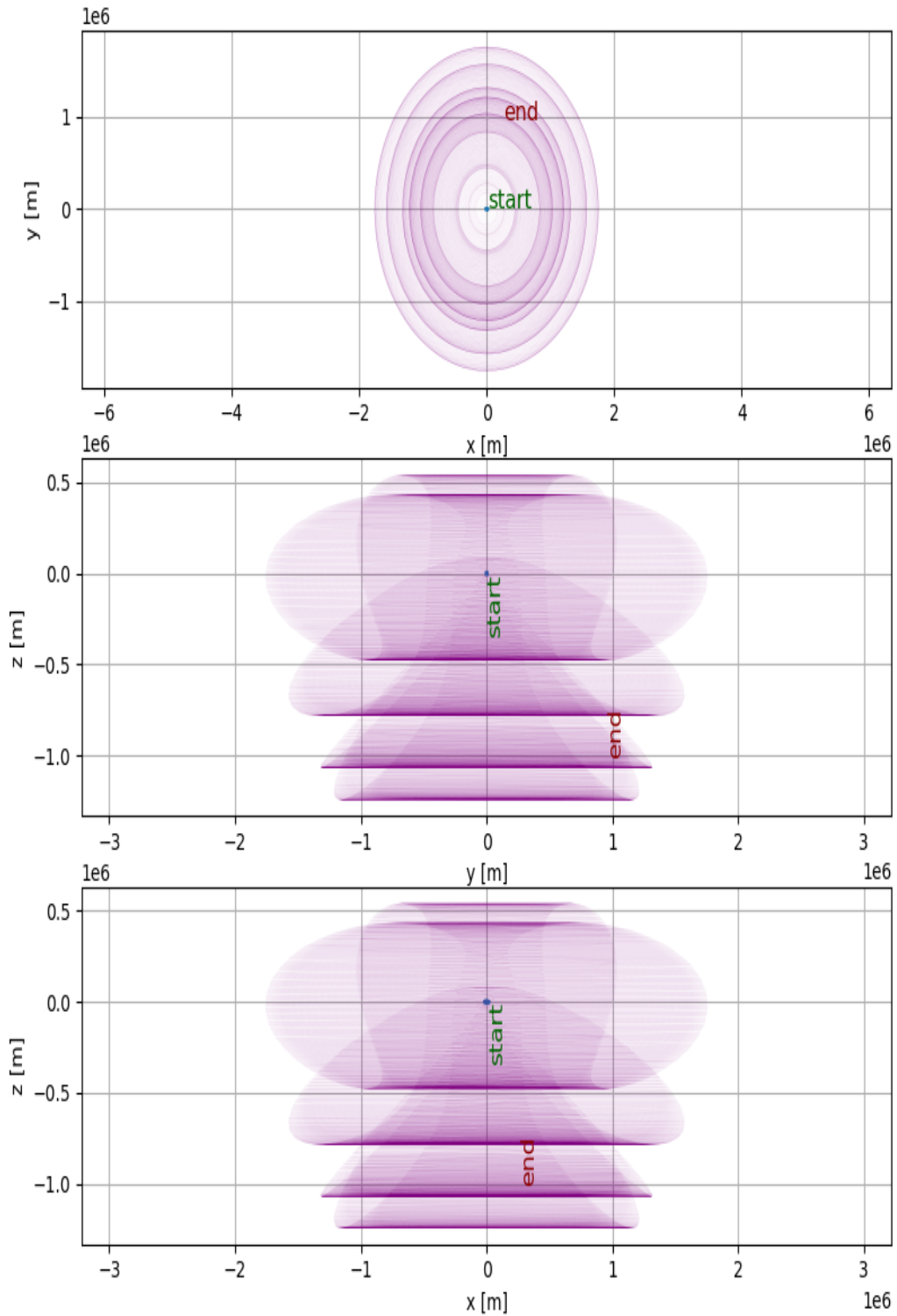**Figure A.5:** 2D rotating frame trajectory of capture regolith for case number 8 in Table 4.2. Particle code LoGSP-1.